1-2018

Collaborative Robotic Path Planning for Industrial Spraying Operations on Complex Geometries

Steven Brown
University of Arkansas, Fayetteville

Collaborative Robotic Path Planning for Industrial Spraying Operations on Complex Geometries

A thesis submitted in partial fulfillment
of the requirements for the degree of
Master of Science in Industrial Engineering

by

Steven Louis Brown
University of Arkansas
Bachelor of Science in Industrial Engineering, 2016

December 2018
University of Arkansas

This thesis is approved for recommendation to the Graduate Council.

Harry Pierson, Ph.D.
Thesis Director

W. Art Chaovalitwongse, Ph.D.
Committee Member

Chase Rainwater, Ph.D.
Committee Member

ABSTRACT

Implementation of automated robotic solutions for complex tasks currently faces a few major hurdles. For instance, lack of effective sensing and task variability – especially in high-mix/low-volume processes – creates too much uncertainty to reliably hard-code a robotic work cell. Current collaborative frameworks generally focus on integrating the sensing required for a physically collaborative implementation. While this paradigm has proven effective for mitigating uncertainty by mixing human cognitive function and fine motor skills with robotic strength and repeatability, there are many instances where physical interaction is impractical but human reasoning and task knowledge is still needed. The proposed framework consists of key modules such as a path planner, path simulator, and result simulator. An integrated user interface facilitates the operator to interact with these modules and edit the path plan before ultimately approving the task for automatic execution by a manipulator that need not be collaborative. Application of the collaborative framework is illustrated for a pressure washing task in a remanufacturing environment that requires one-off path planning for each part. The framework can also be applied to various other tasks, such as spray-painting, sandblasting, deburring, grinding, and shot peening. Specifically, automated path planning for industrial spraying operations offers the potential to automate surface preparation and coating in such environments. Autonomous spray path planners in the literature have been limited to generally continuous and convex surfaces, which is not true of most real parts. There is a need for planners that consistently handle concavities and discontinuities, such as sharp corners, holes, protrusions or other surface abnormalities when building a path. The path planner uses a slicing-based method to generate path trajectories. It identifies and quantifies the importance of concavities and surface abnormalities and whether they should be considered in the path plan by comparing the

true part geometry to the convex hull path. If necessary, the path is then adapted by adjusting the movement speed or offset distance at individual points along the path. Which adaptive method is more effective and the trade-offs associated with adapting the path are also considered in the development of the path planner.

ACKNOWLEDGEMENTS

I would first like to thank Dr. Harry Pierson for his support and guidance over the past few years, without which, I would not be where I am today. His unending passion for robotics and automation has opened my eyes to new possibilities and inspired me throughout my research.

I would also like to thank all of the faculty and staff in the Industrial Engineering department at the University of Arkansas who have helped me throughout the years. At this point, there are too many to count, but I am grateful for every one of them.

I also wish to acknowledge the engineering team at Red River Army Depot for allowing me the opportunity to pursue this idea and to study their processes.

Additionally, I would like to thank Greg Harms for his invaluable work developing the user interface that has made all of the work I've done look good.

Finally, I would like to thank my family and friends for supporting me throughout the process and being there when I need them most. I am beyond grateful for each and every one of you.

TABLE OF CONTENTS

PUBLISHED PAPERS

Chapter 2: Published

S. Brown and H. A. Pierson, “A Collaborative Framework for Robotic Task Specification,” *Procedia Manufacturing*, vol. 17, pp. 270–277, 2018.

Chapter 3: Abstract Under Review

S. Brown, “Adaptive Path Planning of Novel Complex Parts for Industrial Spraying Operations.”

1. INTRODUCTION

When the idea for this research was first conceived, the task was to design an automated pressure washing work cell capable of handling a large majority of the parts present at one of the Army's rework and rebuild depots. This presented a particular challenge due to the vast differences in part size and geometry that needed to be cleaned on a daily basis. The facility is responsible for cleaning pallets of smaller parts, as well as full tank bodies. Further compounding the problem was the realization that there was almost no way of consistently identify the exact geometry of a part. Whether that be from lack of existing data, easy to miss differences between parts or the fact that the process is still manual and most parts are still custom made, especially for rework and rebuild facilities like this one.

In the past, these challenges have deterred most facilities from attempting to automate the process and choosing to do it manually instead. While this is certainly the most common method, the physical toll these jobs take on the people doing them is undeniable and until recently the technology needed to automate these tasks has been relatively inaccessible, whether that be due to cost or the sheer difficulty of the task being automated. Specifically, full coverage path planning is one of the most difficult tasks to automate reliably and economically. Not to say it isn't doable, but most cases where these tasks are automated don't need to build a new path plan for each part. They are typically used to repetitively do the same set of preprogrammed parts over and over again.

Given the knowledge that human operators are very good at making the judgement calls of what needs to really be cleaned and that a generally good path plan can be built on the fly by an automated system, the task became how to blend a human's cognitive function with the precision and endurance of an automated robotic system, an idea pioneered by the collaborative robotics

community. Taking this idea a step further, adaptive path planning was embraced to create a better path than the generally good path created by the naïve path planner. Due to the growing scope of this project, it was broken down into two separate problems. The first being what does the collaborative system look like from the initial input to user verification and ultimately process execution, and the second being what does an adaptive path planner for pressure washing look like. These two problems were answered in two separate papers and have been included as Chapters 2 and 3 of this thesis.

2. A COLLABORATIVE FRAMEWORK FOR ROBOTIC TASK SPECIFICATION

Since the first industrial implementations of robotic solutions in manufacturing environments, task specification has been one of the toughest and most time-consuming parts of the implementation process. As robotics has advanced, so has the technology surrounding task specification; however, there is still a need for the operator to physically program the robot. While this is fine for low-mix, high-volume production processes, it is a very restrictive requirement for the automation of lower-volume processes. Automated task specification would go a long way toward alleviating some of the hurdles faced by high-mix, low-volume processes. However, the implementation of automated robotic solutions for complex tasks currently faces a few major hurdles. Lack of effective sensing and task variability create too much uncertainty to reliably hard-code a robotic work cell. Collaborative robotics have proven effective for mitigating uncertainty by mixing human cognitive function and fine motor skills with robotic strength and repeatability. Yet, there are many instances where physical interaction is impractical, as human reasoning and task knowledge are still needed. The solution is a framework that blends the latest developments in automated task specification with the experience and cognition of a human operator to provide a more accurate task specification. While this chapter does focus on surface finishing tasks such

as pressure washing, sandblasting shot peening, deburring, grinding, sanding, and wire brushing, the framework can also be applied to any robotic task that does not have a predefined path, such as assembly, inspection, packaging, and pick-and-place operations.

The inspiration for this chapter is a pressure washing work cell. The current work cell is an entirely manual operation with the operators being subjected to high ergonomic risk factors [1]. As such, this process is a strong candidate for automation, but high degrees of variability and uncertainty, combined with extremely difficult perception problems (e.g., differentiating black paint from grease) make traditional robotic automation impractical. By designing an automated system to suggest a toolpath for cleaning and then using the operator's intelligence and understanding to inform the automated side of potential changes, the system can consistently handle the variability in the process.

2.1. LITERATURE REVIEW

While there are many well-documented methods, safety measures, and best practices for general robotic implementations, there are few frameworks designed for the challenges and needs of automating a specific task. The most significant research has been in a software-based approach to connect various sensors and actuators together to create complex systems, such as robots, and has resulted in the formation of the open-source Robotic Operating System [2]. While the ROS consortium and others focus on the integration of tools, sensors, and some external software, other research has focused on how robots communicate within themselves [3]. Depending on how intra-robot communication is viewed, this can be interpreted in one of two ways: either by considering each piece of a robot as its own robotic module or by considering a group of similar robots focused on the same task. When considering a modular robot, there are steps that can be taken to design the optimal robot based on the available modules and the needs of the task [4]. While this method

does help when deciding what style or configuration of robots is needed, it does not address anything other than the physical requirements of the task. When considering communication across multiple robots, there are a variety of methods being used to manage the interactions of multiple robots, from linked pathed planners to swarm intelligence [5, 6]. This has predominately been a focus of mobile robotics, especially with the rise of cleaning and delivery robots [7, 8]. With the ability to control multiple robots or parts of a robot independently to accomplish a task, other research has looked at how a distributed system might manage multiple simultaneous requests either by prioritizing certain tasks over others or by attempting to complete multiple tasks at the same time [9]. On the collaborative side, there are some general frameworks for how a robot could communicate with a human, but they are focused around mobile robotics and collision avoidance [10].

Over the past few years there has been a major push in the robotics community toward a new style of robot that can better interact with human operators. Called collaborative robots, or cobots, they are designed to work together with humans to accomplish a task in the most productive way possible by leveraging the strength and endurance of robots with the flexibility and decision making of humans [11]. They are able to do this by integrating new safety standards and methods into this new generation of robots and by refitting systems with older industrial robots to meet the new safety standards as discussed below. These new safety standards have allowed for numerous new automation opportunities, both in how robots are used and where they can be used [12, 13].

Traditionally, whenever an operator needs to physically interact with a robot in any way, they need to use a lock-out procedure to ensure that either the robot's servos are turned off or the robot is locked in place by some other mechanism. With safety-rated monitored stops, this is no longer necessary. As long as the robot does not move from its current position, the operator is free to enter

the workspace without shutting down the robot or going through a lock-out procedure. A hand-guided cobot allows for the operator to directly affect the position of the robot with their hands without deactivating the servo motors. This is especially useful for robotic arms with axes that can be easily affected by gravity and would usually require power to maintain their position. This style of collaboration allows for faster and easier teaching and programming, and allows humans to use the robots to lift the majority of a heavy load while the operator guides it into place. A cobot utilizing speed and separation monitoring allows the operator to move freely throughout the workspace while the robot is in motion, as long as a dynamically defined minimum separation distance is maintained between the robot and the operator; otherwise, the robot will immediately initiate a protective stop. Power- and force-limiting robots are specifically built for physical contact with the operator that can occur both intentionally and unintentionally by limiting the maximum capable applied forces to comply with defined threshold limits [14].

Aside from the physical interpretations of collaborative operation, there are also many human interface changes that can make a robotic implementation collaborative. As discussed above, some of the collaborative operating methods can be used to enhance the programming experience by allowing the human to interact with the robot [15]. While this does not lead to a collaborative operation, it does minimize the time spent on setting up the operation, which can be just as valuable.

2.2. GENERAL FRAMEWORK DESIGN

This section discusses the modules required within the framework as well as reveals the key attributes for the success of each module. Figure 1 illustrates how the individual modules interact with each other, the external components of the system, and the human operator. From a high level, the system takes the provided 3D data and initial user input as parameters into the path planner to

generate a path. The path is then sent to the path analyzer before the simulation displays the original 3D input, the path, and the analysis. From here, the operator can decide to accept the proposed task as is or make adjustments. If necessary, the adjustments are made by the path modifier module and then sent back through analysis before the operator has the opportunity to make another decision. Upon approval, the path is passed to the robot and the task is completed. However, if the operator notices that there are still unsatisfactory spots, the process can be started again with either the full part or a smaller section being passed to the path planning module.

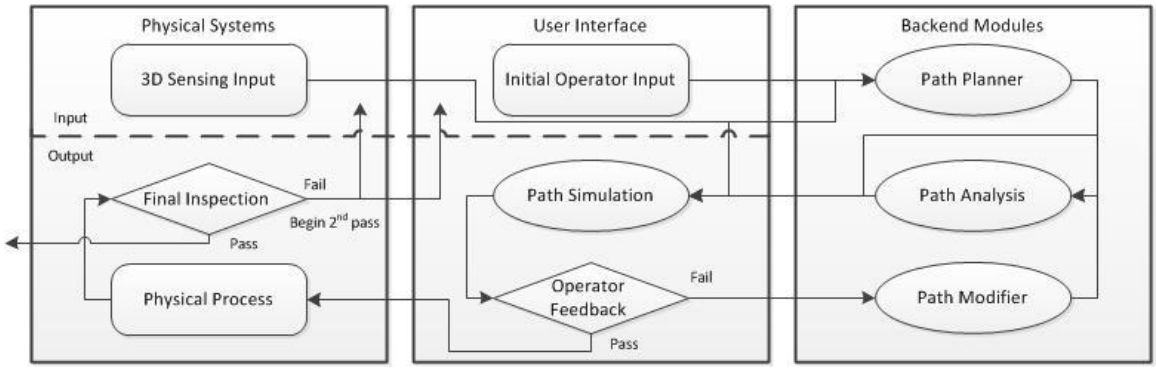

Figure 1: System Framework Design

There are two types of data required for any robotic task specification system: the specific geometry of the object and the parameters of the process being specified. Each type of data can be acquired through various means and faces its own unique issues. For instance, there are a variety of representations of 3-dimensional data, and the data can be easily affected by many environmental variables. The same is true of process parameters. There can be quite different types of parameters that may need to be derived or subjectively chosen by a human operator, which creates another layer of uncertainty. The most important piece of any data collection module or process is that there is a standardized method for doing so that eliminates as much uncertainty as possible.

One might assume that it is feasible to fully automate the process and eliminate a vast majority of the uncertainty, but there are still some large issues surrounding 3D data collection that need to be solved before that is possible for a one-off task specification system [16, 17]. One of the biggest is the need to ensure that the data is completely accurate. 3D sensing technologies can still be easily fooled due to environmental or surface conditions. Lighting plays a huge part in achieving an accurate scan of the part. If a surface is not reflecting the light as the system expects an error may occur in the final rendering. This could ultimately lead to collisions during the task. There is also the possibility that the true part geometry is being obscured by dirt or debris. While this is not problematic in processes such as pressure washing, it can cause challenges in processes such as deburring, where debris could be interpreted as integral to the piece and thus not be removed. Another concern is that the environment or the process itself could cause problems for the sensing mechanism. Any spray, smoke, particles, or general debris being scattered about during the process, along with any additional environmental variable, could obscure or alter the view of the sensors. Covering the sensors to protect them and scanning ex situ both present issues. Not only is it necessary to touch the part twice, but there is the concern about orientation and registration issues once the part is placed in the workspace. Achieving the appropriate orientation and registration of an unfixtured part with no on-site 3D sensing equipment puts a significant burden on the operator to get things exactly right every time.

Other big concerns for the initial data collection are how to ensure that the information provided by the operator is accurate and how to determine the right amount of human interaction required to maintain a flexible yet accurate system. These questions are interdependent. For the right amount of human interaction to be determined, one must understand how much the input can vary based on human judgement and error, and how much that particular input affects the task

specification process. For example, orienting and registering an unfixtured part, as described above, requires the user to match points on the part in the robot's workspace with the same points on the 3D model. This brings in not only error from the operator's judgment about it being "close enough" but also the error in the measuring device used. Finding the right balance between accuracy and usability while maintaining operator support can be difficult. It is important to note that while robotic automation has seen a huge surge in popularity across many industries, only about 10 percent of manufacturing jobs have been automated [18]. Part of that is due to the fact that many workers are less likely to accept robots that completely replace their job without any mistakes. In fact, recent studies show that "clumsy robots" that sometimes need help or make mistakes are better received by humans [19]. This is where collaborative systems can be most beneficial, by allowing limited user control and feedback to inform the robot of what should be done while maintaining a higher level of accuracy and precision.

2.2.1. Path Planner

The path planner has the largest influence on system performance, which is not surprising considering the large amount of work that has already been done in the area. From seed and slicing based models to advanced genetic algorithms, there are multitudes of ways to generate an initial tool path [20, 21]. There are several key factors to consider when designing a path planning module. First, knowing and understanding the process and its requirements is key to building an accurate path planner. The path needed to deburr a surface must be much more precise than the path needed to sandblast that same surface. The controls are also different. A deburring operation needs to control which grinding tool is used and its cutting speed, whereas a sandblasting operation needs to control the type and quantity of sand being used. The sandblasting operation would also be more affected by the excess coverage issues, which places more significance on finding non-

overlapping paths. Another key consideration would be how to link parts of the path with the corresponding area on the surface. This is essential when considering location-specific user input and feedback. Without any way to link areas in need with specific segments, the entire path would need to be rebuilt every time a change is needed to be made. Another staple of a good path planner is robustness to the noise surrounding the part. Depending on the process, this can be achieved by generalizing the original geometry or sometimes ignoring specific pieces during the planning phase. Finally, a good path planner should take into consideration the robot's capabilities when building the final path. A path that may be technically feasible may not be the best path overall due to limits on the robot's reach, joint limits, and singularities.

2.2.2. Path Analysis

The path analysis module provides a measure of how effective the path planner was in achieving the desired results for the process. When designing this module, there are a few key issues. Most importantly, an accurate mathematical representation of the end effector and the process is required. Without this, any generated feedback will be inaccurate. While there are plenty of existing models of various processes, each model relies on input parameters unique to the particular setup. After an accurate process model has been achieved, there should be a methodology defined for quantifying the effect of the process on the surface. For instance, a pressure washing model could be quantified by the cumulative energy impingement on the surface as a function of distance and incidence angle, while a sanding operation could be quantified by the grit of the sander and the pressure applied. These quantifications can then be used to track the overall work done on the surface over time. This process must then be applied to the path. The most reliable method for modeling the entire path is to discretize the path into individual points derived from a consistent time period. After iterating through the entire path, there will be a

corresponding impingement value for all of the affected facets on the surface at each time value. These values can then be summed by facet to create the total impingement value for each facet for the entire path. These final values may then be scaled and trimmed in a way that accurately represents the process. For instance, a pressure washing operation is typically not concerned with overtreating a surface, and path evaluation can consider any value over a given threshold acceptable, whereas sandblasting would require limiting the impingement values to within a certain range. Once the impingement values have been scaled, they can be used to inform a variety of internal and external decisions moving forward based on the requirements of the process.

2.2.3. Path Simulation and User Interface

Assuming all of the above modules are working correctly, none of them output data in a way that is easily comprehensible by the operator, making simulation and the human-machine interface critical. The interface and simulation should be robust enough to allow the human operator to quickly and easily understand what is happening, and allow them to make the appropriate judgements and adjustments. This section will discuss some guidelines for what can be included in this module as well as some novel ways of using the data from the previous modules.

In order to provide the necessary depth of information in simulation, there are three particular pieces of data that should be displayed. First, there should always be a properly oriented and accurate representation of the part. This ensures that the operator knows exactly which pieces correspond to the physical part. However, assuming the operator is using a stationary workstation, there is a point-of-view problem, where the operator can see only part of the object. One solution is to mount a camera on the robot and allow for visual inspection as the robot moves through the path, which could be time consuming. Another solution is to reskin the simulated part with actual images of the part, similar to photogrammetry, which would allow for the most accurate initial

representation. Secondly, the simulation should show the proposed toolpath, as shown in Figure 2a. This is necessary not only to ensure there are no collisions or errant movements, but also to make sure the user understands the possibilities when choosing a method for improving the path. To further improve the simulation, a model of the end effector and the corresponding process should be added. Also, depending on the feedback methods, the displayed path could be selectable and manually editable for more advanced users. Finally, the simulation should also have an efficient way to represent the impingement values that does not interfere with other aspects of the simulation. The easiest way to achieve this is by using the values corresponding to each facet and applying a color scale effect to create a heat map of the process' effectiveness as shown in Figure 2b, where red represents maximum coverage and blue represents no coverage. While this would interfere with the visualization method proposed above, the two could be toggled or have a slightly transparent version overlaid over the other.

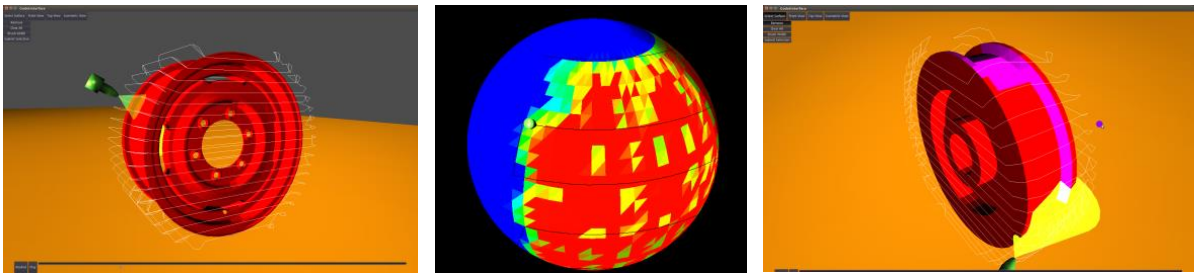

Figure 2: (a) Path with process simulation; (b) Process analysis visualization; (c) User interface with process simulation

Given those three pieces of data, there are certainly plenty of other things that can be done to make the overall simulation environment more intuitive and pleasing for the user. Having intuitive controls for rotation and navigation is a must. Not only do the controls impact the user's opinion of the software and thus their willingness to work with it, but inefficient control schemes can also take up valuable space on the screen. Enhanced visuals and options also go a long way toward

improving the interface. Whether it is as simple as better shading and color choices or advanced options, such as the ability to turn features on and off and customize the interface, anything that makes the overall product feel more polished helps to integrate the user and automation.

Once the user has been given all of the necessary information from simulation, they should be given the opportunity to provide feedback and request further iteration if necessary. This step also has the same pitfalls as the initial user input where the interface needs to provide enough feedback options for effective information gathering, while minimizing the effect the user's subjective opinions have on the end product. While the initial planning algorithm takes into account only the condition of the part as a whole, localized options are much more efficient when creating directions for second-pass modifications. This means that the capability for selecting individual parts of the surface with a high-enough resolution is essential. Figure 2c provides an example of surface selection, the pink colored facets have been selected for some rework or modification. As discussed above, most of the operator's decisions are based on their understanding of part condition, the proposed path, and process simulation results. There is no single, simple answer for displaying all of this information in an integrated fashion. For example, one possibility is to display the original image underneath a faded representation of the impingement values and then completely cover both with a fully opaque color once the facet has been selected. This allows for the operator to see and interpret both datasets before deciding whether to select them. Another opportunity for surface selection is to use statistical grouping techniques to find and classify larger sets of facets that may require additional processing. While this still relies on having a selectable surface, it helps eliminate the resolution issues created by selecting individual facets. Ideally this method would be able to take all of the facets not meeting the requirements of the process and group them into contiguous surfaces of similar impingement values, and then present the operator

with the option to make modifications to each such surface. The specific modification options will be process dependent, but regardless of what changes are made, the operator should always get feedback as to how the changes impact the quality of the specified path before giving the final approval to execute the task.

2.2.4. Path Modifier

As with almost all of the modules above, the path modification module will be very process specific, but there are a few key capabilities needed to be effective for any process. First and foremost, it should not make any changes to the formatting of the data, meaning that any changes made should not affect the other modules' ability to understand them. This is especially important for maintaining version control since there is the possibility that the operator makes a poor choice and makes the planned path worse. One method for maintaining version control is by keeping the original path plan in the planning module, building an entirely new path from it using whatever pieces have been deemed acceptable, and then finally making the necessary changes as the new version is built. However, this can be difficult because it is not always clear what needs to be changed to make the path better: Maybe pieces of the path need to be removed and replaced, maybe the pieces need only to be removed, maybe there need to be additional passes added, or maybe there needs to be a change in the process parameters for that particular piece. This also requires that this module be able to link specific pieces of the path to the facets they effect on the surface and have been selected for modification. One way to do this would be to mark the correlation earlier in the planning process, but that still can leave multiple pieces of path affecting the same facets—thus doing little to make a decision on which one should be modified. Because of this indecision, another possibility for accounting for low impingement values is simply to tack on additional pieces of path for the robot to execute after completing the original path. While this can

certainly work, constantly jumping from place to place means that there is a greater chance for collisions. To combat this issue, there needs to be some collision avoidance logic built into the path modifiers to ensure that everything will flow smoothly. Some potential modifications to the path could include changing the attack angle, slowing down the tool head's movement, replanning for only the problem areas, and adjusting the offset distance for non-contact operations. At the very least, this module should be prepared to be iterated multiple times, making the finer changes to eventually produce a good path plan. In this case, some internal iteration might be preferred so that the operator does not need to keep checking and rechecking all of the time.

2.3. IMPLEMENTATION

In order to realize the distributed nature of the system, the Robotic Operating System (ROS) was used to coordinate communication amongst the nodes in the network. ROS was chosen because it supports multiple languages and since there are no modifications to the data between the languages. This allows a variety of sensors, hardware, software, and various other accessories to communicate easily. It also has convenient methods for managing node executions and version control. For example, a ROS service node holds program execution on the client side until it has completed. This helps to ensure that the current task plan is not being modified by something else when it is accessed by another node.

For a system like this to work, maintaining data integrity is key, especially when all of the newly created data points need to be linked back to the originals. As discussed above, version control and communication between languages are what ROS does well. While most languages use different mixes of lists, arrays, tuples, and various other data structures, almost all languages hold true to the basics such as text strings, integers, and floating-point numbers. ROS is no different, as it supports the basic data types but uses its own structures, called messages. For this framework

system, custom ROS messages were written to accurately represent the data and transfer it between the nodes, where it was translated to and from the native data structures for use.

Currently, the prototype implementation is being built on Ubuntu 16.04 with the majority of the code written in Python 2.7. The GODOT gaming engine is used for simulation and the main user interface. Various open-source python packages are used to handle the rest of the process. As shown in Figure 2, the planned path is visualized along with a representation of the spraying process. The user can then consult the impingement data as displayed on the part and select facets needing rework. Since this is non-contact, the user can choose to modify speed or offset distance to better clean the selected facets, and this process can then be iterated until an acceptable path is found.

Although this chapter focuses on full-part coverage for surface-finishing task specification, the framework can also be applied to tasks with less obvious goals, such as assembly, inspection, packaging, and pick-and-place operations. For these tasks, many of the modules discussed are still useful, but will have different goals and may be utilized in a different order. For the initial data input, the system still needs to understand the pose of all objects, but the input parameters can look different. In some cases, there may not be any input from the operator until a simulation has been rendered. The same can be said of the path planning, analysis, and modification modules. In these tasks, unlike full-coverage path planning, the goal may not be completely clear, since user input could be required before anything other than a simulation of the part and environment could be done. In these cases, an additional module could be added for identifying the task at hand and determining what needs to go where. For instance, a task identifier module could leverage visual and 3D data to identify where each piece fits with the other.

Consider an assembly robot that has been designed to help assemble a wide variety of products. Once the system has been shown all of the parts for the assembly, a task identifier module could make the initial decisions about what goes where before passing on those decisions to the operator to be confirmed or edited. Once the operator gives the go-ahead, the path planner module can take over and make a first pass at determining the appropriate trajectories for the assembly process. The trajectories would then be reviewed by the operator who could then approve them or make edits and suggestions for an improved trajectory. Measuring the goodness of these trajectories could be difficult, especially when considering how to convey the results clearly to the operator, but assembly is a bit more intuitive than finding an optimal surface covering path.

Other additional hurdles for implementing a system for non-surface finishing operations are inevitable because there is no easy and reliable way to fully complete the entire task in simulation before executing. For example, the above assembly trajectories rely on the gripper being able to replicate the grip that was achieved in simulation for the rest of the trajectory to be accurate. An alternative to this problem would be to rescan and replan each step after the robot picks up a piece with its gripper. While this would help increase accuracy, it would add significant time to the process. This also means that the operator needs to keep checking on the simulation throughout the assembly process, which makes the human more of a tele-operator than a supervisor. While that is not necessarily a bad thing and could even be ideal in some industries, it does not do much to improve the operator's efficiency.

2.4. CONCLUSIONS

As robotic technologies continue to advance, so should the way humans can interact with them. Collaborative robotics both physically and virtually are the next step in furthering the integration of robotics into industry and our everyday lives. While it is impossible to know what new

technologies might dramatically shift how we think about robotic implementations in the future, having a framework for collaboration between robots and humans to complete complex and diverse tasks will be essential. The collaborative robotic framework for task specification proposed here is one step toward fully automated systems capable of very high-mix, low-volume manufacturing.

2.5. REFERENCES

[1] A. Woods and H. Pierson, "Developing an Ergonomic Model and Automation Justification for Spraying Operations," in *Proceedings of the 2018 Institute of Industrial and Systems Engineers Annual Conference*, Orlando, FL, 2018.

[2] M. Quigley, B. Gerkey, K. Conley, J. Faust, T. Foote, J. Leibs, E. Berger, R. Wheeler and A. Ng, "ROS: an open-source Robot Operating System".

[3] R. Johansson, A. Robertsson, K. Nilsson, T. Brogard, P. Cederberg, M. Olsson, T. Olsson and G. Bolmsjo, "Sensor integration in task-level programming and industrial robotic task execution control," *Industrial Robot: An International Journal* , vol. 31, pp. 284-296, 2004.

[4] Z. M. Bi and W. J. Zhang, "Concurrent Optimal Design of Modular Robotic Configuration," *Journal of Robotic Systems* , vol. 18, pp. 77-87, 2001.

[5] M. Montemerlo and S. Thrun, FastSLAM: A Scalable Method for the Simultaneous Localization and Mapping Problem in Robotics, Springer, 2007.

[6] G. Beni and J. Wang, "Theoretical Problems for the Realization of Distributed Robotic Systems," in *IEEE International Conference on Robotics and Autanatioo*, Sacremento, CA, 1991.

[7] E. Prassler, A. Ritter, C. Schaeffer and P. Fiorini, "A Short History of Cleaning Robots," *Autonomous Robots* , vol. 9, pp. 211-226, 2000.

[8] A. Martinoli, K. Easton and W. Agassounon, "Modeling Swarm Robotic Systems: A Case Study in Collaborative Distributed Manipulation," *The International Journal of Robotics Research* , vol. 23, pp. 415-436, 2004.

[9] B. Siciliano and J.-J. E. Slotine, "A general framework for managing multiple tasks in highly redundant robotic systems," in *Fifth International Conference on Advanced Robotics*, 1991.

[10] T. Fong, C. Thorpe and C. Baur, "Collaborative Control: A Robot-Centric Model for Vehicle Teleoperation," AAAI, 1999.

[11] A. Djuric, R. J. Urbanic and J. L. Rickli, "A Framework for Collaborative Robot (CoBot) Integration in Advanced Manufacturing Systems".

[12] T. Anandan, "Robotic Industry Insights: Collaborative Robots and Safety," Robotic Inustries Association, 26 Jan 2016. [Online]. Available: https://www.robotics.org/content-detail.cfm?content_id=5908.

[13] P. Waurzyniak, "Putting Safety First in Robotic Automation," *Manufacturing Engineering*, pp. 61-66, September 2016.

[14] S. Brown, A. Woods, H. Pierson and G. Parnell, "An Operations Management Perspective on Collaborative Robotics," in *American Society for Engineering Management International Annual Conference*, Huntsville, AL, 2017.

[15] Robotiq, "Teaching Robots Welding," [Online]. Available: http://robotiq.com/solutions/robot-teaching/. [Accessed 6 May 2017].

[16] F. Remondino and S. El-Hakim, "IMAGE-BASED 3D MODELLING: A REVIEW," *The Photogrammetric Record*, vol. 21, pp. 269-291, 2006.

[17] J. D. Schutter, T. D. Laet, J. Rutgeerts, W. Decré, R. Smits, E. Aertbeliën, K. Claes and H. Bruyninckx, "Constraint-based Task Specification and Estimation for Sensor-Based Robot Systems in the Presence of Geometric Uncertainty," *The International Journal of Robotics Research*, vol. 26, pp. 433-455, 2007.

[18] H. Sirkin, M. Zinser and J. Rose, "The Robotics Revolution: The Next Great Leap in Manufacturing," BCG, 2015. [Online]. Available: https://www.bcg.com/publications/2015/lean-manufacturing-innovation-robotics-revolution-next-great-leap-manufacturing.aspx.

[19] N. Mirnig, G. Stollnberger, M. Miksch, S. Stadler, M. Giuliani and M. Tscheligi, "To Err Is Robot: How Humans Assess and Act toward an Erroneous Social Robot," *Frontiers in Robotics and AI*, vol. 4, p. 21, 2017.

[20] W. Chen and D. Zhao, "Path Planning for Spray Painting Robot of Workpiece Surfaces," *Mathematical Problems in Engineering*, 2013.

[21] A. UGUR, "Path planning on a cuboid using genetic algorithms," *Information Sciences,* vol. 178, pp. 3275-3287, 2007.

3. ADAPTIVE PATH PLANNING OF NOVEL COMPLEX PARTS FOR INDUSTRIAL SPRAYING OPERATIONS

Operations such as spray painting, powder coating, pressure washing and blasting operations make up one of the more common processes in manufacturing across many different industries. When performed by humans, these tasks often require full body safety equipment such as coveralls and face masks, which while they do help combat the safety issues, they can also hinder an operator's ability to work in the environment. For example, in a detergent based pressure washing cell, the operator is subjected to a very hot and humid environment, which translates to a very hot and uncomfortable suit, with spray from the pressure washing obscuring their vision through the mask. The operator's solution to these new problems is commonly to remove their safety equipment. A robotic solution helps bring human operators out of what can be a very dull, dirty and often dangerous environment, especially when considering the ergonomic impact the job can have on a person [1].

While there are a variety of current robotic solutions in use, most only deal with parts of known geometry or place restrictions on the types of geometries that can be serviced. This is especially true in high-volume, low-mix production setting where the part-to-part variance is insignificant. For these instances, quality autonomous path planning is not as critical because the path can be fixed by the operator before execution. This method is impractical for high-mix, low-volume processes, which are becoming more and more prevalent as large manufacturers try to meet the needs of a wider consumer base while maintaining or increasing their efficiency and smaller manufacturers begin to embrace automation as a viable option.

Automated full coverage path planning is nothing new and has been the focus of many research studies. However, there is a lack of depth with regards to dealing with discontinuities, especially

concavities, on the surface. This limits the applications of path planning algorithms and in turn makes it that much harder for agile automation that could benefit many novel low volume operations by allowing for faster reprogramming or requiring no reprogramming at all. This becomes even more important as new breakthroughs in the robotics community, such as collaborative robotics, are making it much cheaper, safer and easier to implement robotic solutions where automation is possible.

The adaptive path planner described in this research was built to drive a robotic pressure washing system that handles a massive variety of novel parts with almost no consistent or anticipatable demand. The path planning method was designed to handle any part of any complexity that delivers a realistic path plan tailored to the specific part that can be executed relatively easily by any industrial robot. While the specifics of the implementation are modeled after a pressure washing process, the broader method can be applied to a variety of robotic tasks that need to be specified on the fly and with minimal operator interaction and correction. In the case of higher volume processes, this could be used as a better stepping off point for human iteration. Furthermore, this research also considers what adaptive methods work best and the trade-offs associated with adapting the path.

3.1. LITERATURE REVIEW

3.1.1. Path Planning

There is plenty of literature available on how to effectively generate a toolpath for robotic spraying applications from CAD data. There has been some research done on parametric CAD data, but the majority of the research has been focused around tessellated mesh files, STL being one of the most common and simplistic file types [2]. Tessellated mesh files have proved popular enough that similar representation methods have been adopted for mobile robotic mapping [3].

When using tessellated mesh files, there are a few different methods for creating the toolpath, but most utilize some sort of slicing algorithm to divide the part up into smaller strips that can be covered by a single pass of a sprayer. One of the simpler implementations of slicing for path planning relies solely on the surface normal at points along the slice to generate a toolpath for the sprayer [4]. This can create problems if the slice is close to a dramatically different surface feature that would not be covered with the particular orientation. One group combats this by generalizing the toolpath by taking a seed triangle and then iteratively adding more triangles who's surface normal meet the desired deviation angle to create a patch. Once no new triangles can be added or the patch is about to exceed the size of the sprayer's coverage area, the patch is complete and so is the tool point for that patch. Multiple patches are then combined to define the full toolpath of the entire surface [5]. Others have taken this a step further in terms of generalizing the toolpath. By taking the approximate surface normal of the patch and creating a bounding box in the same orientation of the surface normal, the 2D side of the bounding box can be sliced to generate a toolpath for that path [6]. One of the new state of the art methods being utilized to handle the complexities of toolpath planning for complex shapes is a dual robot system where one robot manipulates the object and changes its orientation throughout the process to help make the spraying robots toolpath easier to achieve and thus improving time and efficiency [7].

Once any of the above methods has created the points required to appropriately cover the part, deciding on an optimal path is the next step and can be achieved through a variety of statistical and mathematical methods that are more often relied on by the mobile robotics community, such as landmark-based topological coverage, spanning trees, approximate cellular decomposition and spiral filling algorithms amongst others [8, 9]. Neural networks have also been implemented to help deal with uncertainties and sharp corners in the 2D world of mobile robotics [10, 11, 12].

While there isn't as much of a precedent for these techniques in single use path planning, a system that sees enough of the same or similar parts could do very well. Alternatively, genetic algorithms have been used to solve 3D problems similar to the traveling salesman problem created by the toolpath points [13]. As far as adaptive planning methods go, there has been plenty of research done on mobile robotic navigation and multi-robot collision avoidance [14, 15]. However, the research focused on the actual path is mostly focused around probabilistic roadmap planners, which do return the best path to cover all of the defined nodes, but they do not consider the consider the process being modeled or how changes to the path may affect the results [16].

Most previous research only considers parts that are generally convex and continuous with only mild exceptions. There is a need for planners that consistently handle concavities and discontinuities, such as sharp corners, holes, protrusions or other surface abnormalities when building a path. One method designed to plan for unknown parts, relies on 3D sensing and a library of predefined geometries to accurately build the toolpath [17]. This could be improved upon by using predictive probabilistic sensing methods as seen in some mobile path planning applications [18]. However, these methods are only as good as the sensors they employ. This is problematic because there are still many inherent flaws with 3D sensing technologies, despite massive improvements in the field [19, 20, 21]. Among the most prevalent remaining issues are the uncertainties around how a system interprets different textures and finishes, poor lighting and whether or not the sensors have full access to the entire part geometry [22, 23, 24]. For contact methods, such uncertainties can be detected by physical sensors attached to the robot based on defined constraints [25, 26].

3.1.2. Process Simulation

The other piece of this system, the accurate modeling of the process, which for this implementation is spraying operations, has been well studied and has a generally accepted method for doing so. All spraying simulations take into account a variety of factors, such as pressure, distance, angle of attack and surface finish requirements as a bare minimum. These basic variables can be used as a crude, but mostly accurate, representation of the process for most purposes, but the bulk of the academic work has been focused on fine tuning these simulations even further by considering the most minute of variables. These variables can be used to model how the spray interacts with the air around it, the physical properties of the liquid being sprayed, how the physical setup of the sprayer system affects the spray, and the distribution of sprayer strength at a given distance and width along with many others [27]. Taking it a step further, the detailed simulation can be applied across the entire part in a time based cumulative method that helps to account for the total work done across the surface of the part instead of just in one moment [28]. Beyond that, others have looked at how to optimize the path parameters to create a consistent level of work done across the entire part [29]. While building the optimal toolpath seems like the likely pinnacle of a path planning algorithm, the above works do not delve into how to handle the extreme complexities presented in many parts.

When measuring the effects of certain process parameters, the offset distance has been repeatedly proven to be one of the most effective parameters in controlling the amount of work done. This applies to both the amount of pressure applied, but also the effective spraying width at certain distances due to the highly nonlinear nature of distance in spraying operations [30]. At a certain point, the increase in effective sprayer width is rendered moot as the sprayer no longer exhibits an appropriate amount of work required to affect the surface of the part [27]. Furthermore,

with regards to time applied, there will eventually be a steady state achieved where the part can still be within the effective range of the sprayer, but no more cumulative work can be achieved despite multiple passes [31]. With this in mind, this research will only consider time if distance has been adapted and more work still needs to be done.

3.2. METHODS

This approach involves taking some initial 3D data, given as an STL file in this case because the algorithm requires normal vector, and building a convex hull around it to eliminate the collision and accessibility issues created by non-continuous and concave surfaces. However, given a method for determining normal vectors and building a tessellated mesh from a point cloud, any number of 3D data gathering methods could be used. At this point, the mesh is converted into a point cloud where the centroid of each facet is linked to the normal vector of that facet. The path is then built based on the convex hull using a slicing based method that relies on the following input parameters: a rotation axis and the degrees of rotation, which serve to modify the slicing direction, as it is unlikely that the part will actually be moved if the scanner is calibrated and registered correctly; and a slice thickness, an offset distance, and an overlap percentage, which serve to quantify how much work will be applied to the part. Once the path has been built, the points from the original mesh, now represented as a point cloud, are mapped to specific segments of the path. In some cases, a point can be mapped to multiple segments. The individual segments of the path are then adapted based on the points mapped to each segment. The adaptive phase considers the true geometry and will either modify the path to be closer to the part or it will slow the end effector down to facilitate more cleaning power applied to a particular area. From an experimental point of view, the system was used to test two factors; the type of adaptive algorithm used and the statistical aggregation method used within the adaptive algorithm. The user can choose between a time

adapted path and a distance adapted path with the option to also use both or neither adaptive algorithm and a choice of mean, mode, min and max is provided for the aggregation method. The process is illustrated in Figure 1.

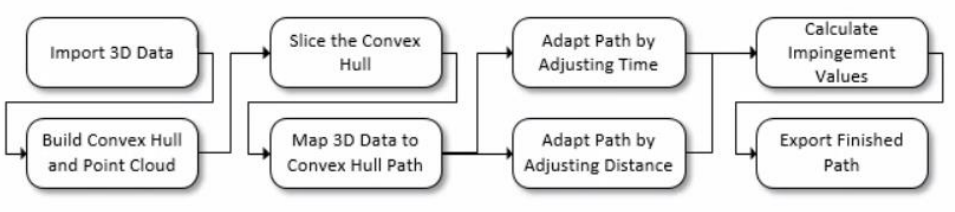

Figure 3: Overview of the Adaptive Path Planner

Outside factors aside and without any adaptive methods, slice thickness, w_A, and offset width, w_O, are the two parameters that most significantly affect the algorithm's performance, but they can be derived from a variety of other measurements based on the specific process. For the proposed spraying process, the slice thickness can be calculated using simple right-angle trigonometry from the angle of the sprayer, θ, and the end effectors distance from the part surface, referred to as the offset distance, d_O. The offset width is calculated as a percentage of the slice thickness based on the provided overlap percentage, σ. Figure 2 illustrates these calculations as well as how the slices can overlap on the surface of the part itself. Base velocity and sprayer intensity can also be provided, but they only serve to augment the results equally and have no effect on the distribution of work done.

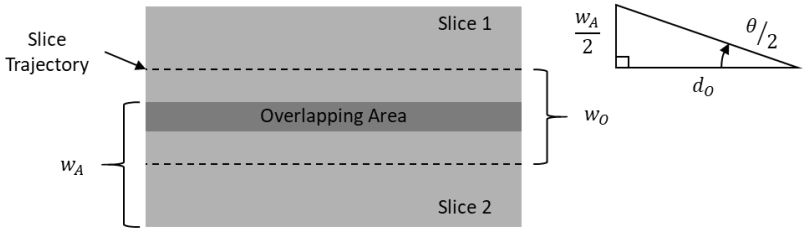

Figure 4: Overlapping Slice Paths and Input Parameter Derivation

3.2.1. Tool Path Trajectory

In order to better understand the path generation process, the form of the finished trajectory is presented here first. After the algorithm has run its course, the initial 3D data has been taken and converted into a final toolpath with seven data points for each position in the trajectory. The first three points represent the X, Y and Z positions of the end effector relative to the center of the part, in this case the origin. These values would need to be translated for any real implementation, but that translation is entirely dependent on the specific implementation. The second three points represent the orientation of the end effector as a directional vector from the end effector to the part, which is found by taking the inverse of the corresponding facets normal vector. This vector can be converted to any other representation as needed. While this vector does not fully define the pose of the end effector, as the rotation about the tool is not addressed, it does allow motion planners a free parameter to find a kinematic solution. This can change based on the process, but assuming a conical spray pattern, this free parameter does not have any effect on the process. The seventh point represents the timestamp of that particular point, which can be used by a robot to generate a trajectory. Each path point is defined as,

$$\boldsymbol{p} = [x, y, z] \tag{1}$$

and each orientation is defined as,

$$\boldsymbol{r} = [x_{\mathrm{r}}, y_{\mathrm{r}}, z_{\mathrm{r}}] \tag{2}$$

and the finished trajectory is defined as,

$$G = \{ [\, \boldsymbol{p}_k \,,\ \boldsymbol{r}_k \,,\ t_k \,] \mid \ \forall\ k = \{0, \dots, \beta\} \} \tag{3}$$

where β is the number of observations in *G*, *P*, *R* and *T*, *P* is the ordered set of all path points $\boldsymbol{p}$, *R* is the ordered set of all orientation vectors $\boldsymbol{r}$, and *T* is the ordered set of all time values *t*.

3.2.2. Slicing the Part

The algorithm builds the path in a similar fashion to additive manufacturing processes. The main difference is that when an additive manufacturing process slices a part, it is slicing to build a solid piece, which needs many thin slices with an interior raster pattern, whereas this process is slicing for exterior surface coverage, which uses a few thick slices without the interior raster pattern, just the exterior perimeter. Throughout this process, all of the slicing and path building action are taken with regards to the convex hull of the part. The original part data is used to inform the adaptive algorithms and all analysis is done using the original part as well. The appropriate number of slices for the convex hull is defined as,

$$m = \lceil (Z_{\max} - Z_{\min})/w_{\mathrm{O}} \rceil \tag{4}$$

where Z_{max} and Z_{min} are the extreme values in the Z axis of the part and w_O is the offset width. The offset width, which represents the distance between each slice, is redefined so that the slices are equally spaced along the entire part, which can be defined as,

$$w_{\mathrm{O}} = (Z_{\max} - Z_{\min})/m \tag{5}$$

This ensures that there is total coverage of the part and can be modified to create overlap on the edges of the part if necessary. The height h_s of each slice *s* is defined as,

$$h_s = Z_{\max} - \frac{w_{\mathrm{O}}}{2} - s w_{\mathrm{O}} \qquad \forall\, s = \{0, \cdots, m\} \tag{6}$$

where *s* is the slice index and $\frac{w_O}{2}$ represents the offset needed to shift the slice from the edge to the center of that slice. For each slice, *s*, the process described in the following sections is repeated until all slices have been planned for and the slices are combined into one complete path.

3.2.3. Path Building on the Slice

Within each slice, which are represented as planes defined by $Z = h_s$, the intersecting facets F_s of the convex hull *H* are found by,

$$F_s = \{f \mid u_f = 1 \ or \ u_f = 2\} \qquad \forall f \in H \qquad (7)$$

where u_f is the number of vertices above the slicing plane defined by,

$$u_f = \sum_{i=1}^{3} \begin{Bmatrix} 1 & , \boldsymbol{q}_{fiZ} \geq h_s \\ 0 & , \boldsymbol{q}_{fiZ} < h_s \end{Bmatrix} \qquad \forall f \in H \qquad (8)$$

where $\boldsymbol{q}_{fiZ}$ is the Z value of vertex *i* of facet *f* on the convex hull *H* and h_s is the height of slice *s*. If a facet has one vertex above or below the plane and the other two are on the opposite side it is considered to be an intersecting facet and is included in the set. When a facet is sliced directly on a single vertex, it is included as is and the following interpolation is not necessary.

When a facet is sliced, there are two intersecting points $\boldsymbol{a}_{fi}$ along the border of the facet that can be interpolated as illustrated in Figure 3. These interpolated points are defined as,

$$\boldsymbol{a}_{fi} = \boldsymbol{q}_{fA} - e_{fi}\boldsymbol{\phi}_{fi} \qquad \begin{matrix} \forall f \in F_s \\ i = \{1,2\} \end{matrix} \qquad (9)$$

where $\boldsymbol{q}_{fAi}$ is the lone vertex on one side of the slicing plane, the interpolation percentage is defined as,

$$e_{fi} = \frac{(q_{fAZ} - h_s)}{\phi_{fiZ}} \tag{10}$$

and the vector between the lone vertex and the other two vertices $\boldsymbol{\phi}_{fi}$ is defined as,

$$\boldsymbol{\phi}_{fi} = \boldsymbol{q}_{fA} - \boldsymbol{q}_{fBi} \tag{11}$$

where $\boldsymbol{q}_{fBi}$ represents the two other vertices, f is an intersecting facet on the convex hull in F_s, and i is the iterator for both sides of the facet that intersect the slicing plane.

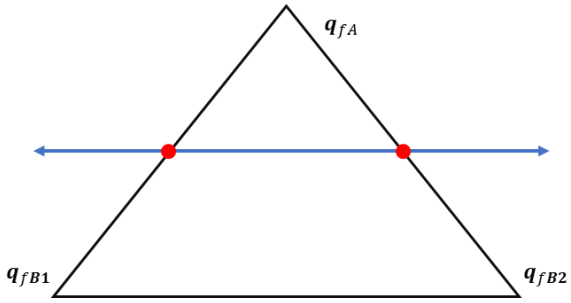

Figure 5: Slicing of an Intersecting Facet

Slicing of the part like this to generate a path does cause some issues that need to be rectified as the planner is slicing or immediately afterward. Each facet generates two points when sliced, one for each side of the facet being intersected and due to the general conventions of tessellated meshes requiring all facets to share each side with another facet, every point is duplicated on the surface polygon at least once. This duplication of surface polygon points and the comparison between their normal vectors is the basis of the two extreme cases that can cause issues; colinear points, identified by similar normal vectors, and sharp corners, identified by very different normal vectors.

Let $A = \{\boldsymbol{a}_i\}$ denote the ordered set of unique surface points generated from Eq. (8) for slice s. These points represent the vertices of a convex polygon in the plane $z = h_s$ that circumscribes the convex hull. They are offset outward from the center of the convex polygon to form the (x,y,z)

elements of the tool path for the slice, P_s, as illustrated in Figure 4. Let $N_i = \{\hat{\boldsymbol{n}}_j\}$ be the set of unique normal vectors associated with the convex hull facets adjacent to $\boldsymbol{a}_i$. The offset path for the slice, P_s, is then defined as,

$$P_s = \{\boldsymbol{p}_k | \boldsymbol{p}_k = \boldsymbol{a}_i + d_o \hat{\boldsymbol{n}}_j \quad \forall\ i,j\} \tag{12}$$

When defining N_i to be a set of unique vectors, the two cases mentioned above need to be dealt with. These cases can be identified by looking at the dot product of the two vectors as,

$$\begin{Bmatrix} |(\boldsymbol{n_j} \cdot \boldsymbol{n}_{j+1}) - 1| \leq \boldsymbol{\varepsilon}, & \text{Duplicate Points} - \text{ See Equation 14} \\ |(\boldsymbol{n_j} \cdot \boldsymbol{n}_{j+1}) - 1| > \boldsymbol{\varepsilon}, & \text{Sharp Corner} - \text{ See Equation } 15 - 17 \end{Bmatrix} \tag{13}$$

where $\boldsymbol{\varepsilon}$ is a value between 0 and 2, which map to $0°$ and $180°$ respectively, that represents the limit of deviation between two normal vectors. In this research, $\boldsymbol{\varepsilon} = 0.05$, which is approximately $4.5°$. For duplicate points, the resulting normal vector is defined as,

$$N_i = \{\hat{\boldsymbol{n}}_{new} \mid \boldsymbol{n}_{new} = \boldsymbol{n}_j + \boldsymbol{n}_{j+1}\} \tag{14}$$

This returns a single vector, $\hat{\boldsymbol{n}}_{new}$, that represents the average of the normal vectors, which is necessary because similar, but not absolutely identical normal vectors are considered unique.

In the case that the shared points have very different normal vectors there is some concern that the resulting toolpath will cut corners and not maintain a very accurate offset distance. To alleviate this issue, intermediary points can be added to the path to help smooth the curve and ease the strain on the robot if the original path requires a drastic change in orientation. The set of normal vectors is then redefined as,

$$N_i = \left\{\hat{\boldsymbol{n}}_l \;\middle|\; \hat{\boldsymbol{n}}_l = \boldsymbol{n}_j + \frac{l}{m}(\hat{\boldsymbol{n}}_{j+1} - \hat{\boldsymbol{n}}_j)\ ,\ \ l = \{0, \dots, m\}\right\} \tag{15}$$

where $\hat{\boldsymbol{n}}_l$ is the new normal generated for intermediary point *l* between normals $\hat{\boldsymbol{n}}_j$ and $\hat{\boldsymbol{n}}_{j+1}$, and m is the number of segments needed to meet the limit ε and is defined as,

$$m = \left\lceil \left| \left(\boldsymbol{n}_j \cdot \boldsymbol{n}_{j+1} \right) - 1 \right| / \varepsilon \right\rceil \tag{16}$$

From these points a coherent toolpath is created by ordering the offset points by the angular coordinate of their polar representation in the XY plane as shown in Figure 4. This is dependent on the part being centered on the origin where the absolute values of the minimum values in each axis are equal to the maximum values.

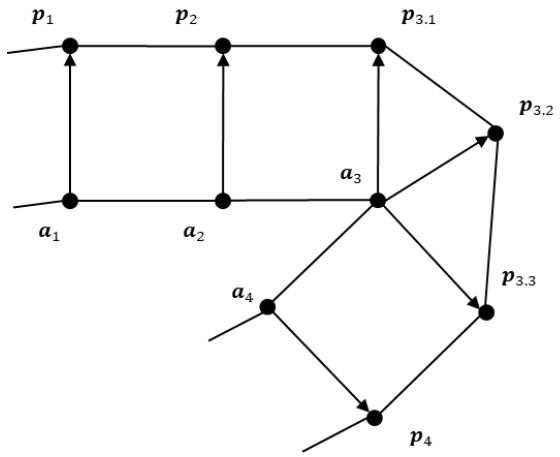

Figure 6: Ordered Toolpath

Additionally, the path is also checked for consistent segment sizes as illustrated in Figure 5. Given the unknown nature of the 3D data and especially with the way convex hulls are built, where flat surfaces are represented by the smallest number of facets required, some facets can be quite large. This results in path segments, which will later be redefined as bins, that may capture too many data points to be effectively adapted. However, before dealing with too large path segments, too small segments are combined into one segment that can be broken up later if necessary.

Let $\Phi_s = \{[\boldsymbol{p}_k, \hat{\boldsymbol{n}}_k]\}$ denote the ordered set of all points and their corresponding normal vectors in the path for slice *s*. Let $\Xi_k = \{\varphi_j\}$ denote the set of consecutive adjacent points that are colinear to point $\boldsymbol{p}_k$, which includes φ_k. These colinear points can be defined in the same manner as the duplicate points in Equation 13. If there are more than two colinear points, since any two points are colinear, all of these points are removed from the path and two new points with new normal vectors are defined as,

$$\Phi_{\text{new}} = \begin{Bmatrix} \varphi_{\text{first}_k} \mid \varphi_{\text{first}_k} = [\boldsymbol{p}_{\text{first}_\xi}, \hat{\boldsymbol{n}}_\xi] \\ \varphi_{\text{last}_k} \mid \varphi_{\text{last}_k} = [\boldsymbol{p}_{\text{last}_\xi}, \hat{\boldsymbol{n}}_\xi] \end{Bmatrix} \forall\, k \tag{17}$$

where $\boldsymbol{p}_{\text{first}_\xi}$ is the first colinear point in the colinear set ξ, $\boldsymbol{p}_{\text{last}_\xi}$ is the last colinear point in ξ, and $\hat{\boldsymbol{n}}_\xi$ is the average normal vector of all points in ξ, which is defined as,

$$\hat{\boldsymbol{n}}_\xi = \sum_{\forall\, j} \hat{\boldsymbol{n}}_j \tag{18}$$

where $\hat{\boldsymbol{n}}_j$ is the normal vector of pair φ_j in the set Ξ_k.

When breaking larger segments down to the appropriate size, the number of segments in the slice is defined as one less than the number of points in the path and the iterator *i* ranges from 0 to the number. Segment sizes are checked and the number of additional points needed for segment *i* is defined as,

$$k_i = \left\lfloor \frac{l_i}{l_{\text{m}}} \right\rfloor \tag{19}$$

where l_i is the actual length of segment *i* and l_m is the maximum allowable length. The new segment length resulting from the additional points is defined as,

$$l_{\text{new}_i} = \frac{l_i}{k_i + 1} \tag{20}$$

The new points being added to the path and the resulting path are defined as,

$$P_{\text{new}} = \left\{ \boldsymbol{p}_{\text{new}_j} \mid k_i > 0\,,\ \boldsymbol{p}_{\text{new}_j} = \boldsymbol{p}_i + \hat{\boldsymbol{v}}_i l_{\text{new}_i} j \quad j = \{1, \cdots, k_i\} \right\} \quad P_s = P_s \cup P_{\text{new}} \quad (21)$$

where P_s is the set of all points in slice *s*, $\boldsymbol{p}_{\text{new}_j}$ is one of *j* intermediary points being added to the path in bin *i* , $\boldsymbol{p}_i$ is one point in segment *i* and $\hat{\boldsymbol{v}}_i$ is the unit vector between $\boldsymbol{p}_i$ and $\boldsymbol{p}_{i+1}$**,** the other original point in the segment. The points are again reordered according to their polar coordinates.

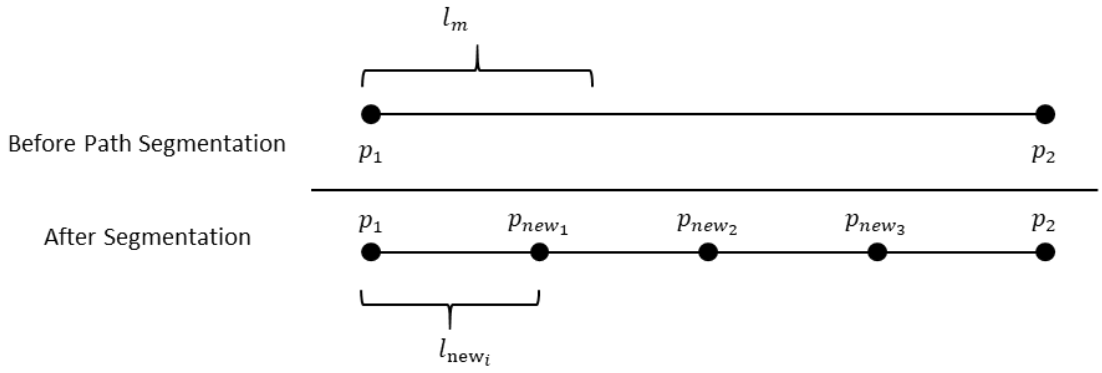

Figure 7: Path Segment Size Control

This produces a geometrically finalized toolpath for slice *s* as shown in Figure 4, excluding the inversion of the normal vector to properly represent the end effectors orientation. However, each data point is still lacking the seventh data point, the time to move between points, needed for a full representation of the trajectory. The resulting trajectory for the slice is defined as,

$$G_s = \left\{ \left[\boldsymbol{p}, \hat{\boldsymbol{n}}_p, \Delta t_p \right] \mid \Delta t_p = d_p / v_0 \quad \forall\ \boldsymbol{p} \in P_s \right\} \quad (22)$$

where Δt_p is the time to move from $\boldsymbol{p}_{x-1}$ to $\boldsymbol{p}_x$, d_p is the distance between the two points, $\hat{\boldsymbol{n}}_p$ is the normal vector corresponding to point $\boldsymbol{p}$, and P_s is the ordered set of all path points on slice s. It should be noted that the time to move to the first point in the path, $\boldsymbol{p}_0$, is zero.

3.2.4. Full Path Concatenation

When adding each slice's path to the master path, there are a few extra pieces needed to ensure a quality path. In this instance, a raster pattern is created by alternating the order with which the points from the individual slices are added to the path, as illustrated in Figure 6. This is useful for robots with limited reach, so that the path does not require the robot to continuously circle the part. To achieve this, the algorithm has ordered the path from the lowest angular polar coordinate to the highest and the points are added in this order for the first slice, and then from highest to lowest in the next and so on. Another method not covered above is the transition from slice to slice. To ensure that there are no collisions with the convex hull in between slices, the part must be sliced using virtually the same method described above, but instead of slicing on the Z axis, it slices on the Y axis. Since this is used only for the transition between slices, and the slices are ordered by the angular component of their polar coordinate, the part should be sliced on the plane where Y = 0 and all facets with negative X values should be thrown out. This assumes that the reference vector for the polar coordinate system is *(1,0).* Using the points generated from this method, the algorithm takes only the points in between the two slices, orders them based on their Z axis values, and then adds them to the path in between the two slices. This could also be modified to generate a path based on a specific angular polar coordinate by redefining the plane as an equation instead of an absolute value in one axis.

After all of the slices have been added and the path is complete, it still needs to be converted into a timestamped path as opposed to its current format with only the time required for each move being reported and the normal vectors need to be inverted to represent tool orientation. A final timestamping method is used return the appropriate timestamps which are defined as,

$$G_{master} = \left\{ [\boldsymbol{p}_g, \boldsymbol{r}_g, t_g] \middle| \begin{cases} g = 0\,,\ t_g = 0 \\ else\,,\ t_g = t_{g-1} + \Delta t_{g-1} \end{cases} \right\} \quad \forall\ \boldsymbol{g} \in G_{master} \tag{23}$$

where t_g is the timestamp of pair g, Δt_{g-1} is the time needed to move from $\boldsymbol{p}_{g-1}$ to point $\boldsymbol{p}_g$, G_{master} is the ordered set of all observations in the entire trajectory, and $\boldsymbol{r}_g$ is the toolpath orientation vector for observation g, which is defined as,

$$\boldsymbol{r}_g = -\hat{\boldsymbol{n}}_g \tag{24}$$

where $\hat{\boldsymbol{n}}_g$ is the corresponding normal vector of observation g identified earlier. This is where the algorithm turns a list of points into a time-based trajectory for a robot to realistically follow. The finished path is then passed on to a either the user for review or the robot itself for execution.

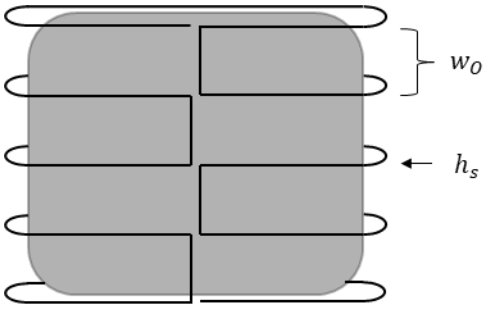

Figure 8: Raster Path Concatenation

3.2.5. Partial Path Creation

In some instances, a full path plan may not be necessary. A user could have pre-existing knowledge of the parts condition and only need to plan for a specific area, or the user could observe some flaws in the original path plans simulation and opt to add an additional partial path to address the issue. Partial path planning can also be utilized to prevent robotic accessibility issues, such as singularities, collisions, and reach issues. Previous research lays out a framework

and infrastructure for facilitating these decisions by allowing the user to select individual facets on the part for partial path planning [38]. In these scenarios, this path planner uses the extreme values of the selected facets Z values and angular components of the centroids polar coordinate to select the necessary parts of the path. Aside from the selection process, the algorithm proceeds as normal. The slices selected as part of the partial path are defined as,

$$S_{part} = \{s \mid Z_{c_{\min}} \leq s_Z \leq Z_{c_{\max}} \wedge s \in S\} \tag{25}$$

where $Z_{c_{min}}$ and $Z_{c_{max}}$ are the minimum and maximum Z values of the selected facets and s_Z is the Z value of slice *s*. Within each selected slice, the planner defines the path points to be selected as,

$$P_s = \{\boldsymbol{p} \mid \varphi_{\min} \leq \varphi_{\boldsymbol{p}} \leq \varphi_{\max} \wedge \boldsymbol{p} \in P_s\} \tag{26}$$

where $\varphi_{\boldsymbol{p}}$ is the angular polar coordinate of the path point $\boldsymbol{p}$, and $\varphi_{\min}$ and $\varphi_{\max}$ are the extreme angular polar coordinates of all of the selected facets. The user is then given the opportunity to again observe the resulting path and make any additions if necessary.

While this method is relatively easy to implement, it is computationally inefficient. An alternative method would be to define a partial convex hull of only the selected facets and then run the algorithm as usual with the partial hull. If a partial convex hull is implemented, there needs to be some methods developed to ensure that the resulting path does not violate the convex hull of the entire part, otherwise a collision is very likely for non-continuous selections and even a possibility for continuous selections. Specifically, since a convex hull is built without regards to the orientation of the original facets inside the convex hull, so the resulting toolpath would still wrap completely around the new convex hull even if the selected facets were only on one

side. The only way to then avoid the method utilized in this planner, would be to successfully link facets on the convex hull to facets on the original point and build a partial convex hull from only the corresponding facets.

3.2.6. Adaptive Methods

To this point, all path planning has been done on the convex hull. This will henceforth be referred to as the "naïve" tool trajectory since it does not consider the underlying surface topology. The following sections describe methods for adapting the naïve trajectory based on the actual part surface. This is accomplished by associating features of the underlying surface with segments of the toolpath and adjusting the tool offset distance and/or velocity based on aggregate descriptions of the underlying surface's position and orientation with respect to the convex hull.

The true surface is represented by a set of ordered pairs of points and normal vectors, $C = \{\boldsymbol{c}, \hat{\boldsymbol{n}}\}$. The points are sampled from the workpiece's tessellated mesh, and each point is paired with the unit normal vector of the facet from which it was sampled. To avoid ambiguity regarding the unit To this point, all path planning has been done on the convex hull. This will henceforth be referred to as the "naïve" tool trajectory since it does not consider the underlying surface topology. The following sections describe methods for adapting the naïve trajectory based on the actual part surface. This is accomplished by associating features of the underlying surface with segments of the toolpath and adjusting the tool offset distance and/or velocity based on aggregate descriptions of the underlying surface's position and orientation with respect to the convex hull.

The true surface is represented by a set of ordered pairs of points and normal vectors, $C = \{\boldsymbol{c}, \hat{\boldsymbol{n}}\}$. The points are sampled from the workpiece's tessellated mesh, and each point is paired with the unit normal vector of the facet from which it was sampled. To avoid ambiguity regarding the unit normal, points should not be sampled from facet edges.

Sampling strategy is a tradeoff between resolution and computational load, and it has implications for how each surface facet influences the adjusted tool trajectory. A simple method is to take the centroid of each facet. This insures that each facet is represented in the ensuing calculations but has disadvantages when facet size varies significantly or facet aspect ratios are high: Areas of high curvature (many small facets) can dominate areas of low curvature (fewer, larger facets), and the centroids of high-aspect-ratio facets can be far from their associated vertices. The disadvantages may be mitigated by enforcing a uniform sampling resolution within facets; however, this can significantly increase the number of points and thus the computational load. A third option is to densely sample the mesh and then down sample via a voxel grid filter (VGF) [39]. The VGF overlays a three-dimensional grid onto the point cloud; all points within each voxel are represented their centroid and normal vectors are represented by their average. The resolution versus computation tradeoff is managed by setting the grid size, though the VGF itself consumes computational resources. For simplicity, and without loss of generality, this research uses the first method – representing each facet via its centroid.

Associating elements of *C* with segments of the slice polygon on the convex hull is done slice-wise. Let

$$C_s = \left\{ \boldsymbol{c}, \hat{\boldsymbol{n}} \mid Z_{s_{\min}} \leq c_Z \leq Z_{s_{\max}} \right\} \qquad \forall\ c \in C \tag{27}$$

be the elements of *C* associated with slice *s*, where c_Z is the Z coordinate of point *c* and $Z_{s_{\min}}$ and $Z_{s_{\max}}$ are defined as,

$$Z_{s_{\min}} = h_s - \frac{w_A}{2} \qquad Z_{s_{\max}} = h_s + \frac{w_A}{2} \tag{28}$$

Ideally, all points, $c \in C_s$, within the volume swept by the spray cone as it moves from point p_i to p_{i+1} would be mapped to that toolpath segment; however, this is computationally expensive both in terms of mapping points and the subsequent calculations where points are associated with multiple segments. Instead, this research opts for a binned approach, whereby each point is assigned to a single segment according to its polar coordinate relative to the origin, as in Figure 7. This assumes that the part has been centered on the origin, otherwise the centroid of the convex polygon could be used in its place. It is further required that the surface facet(s) represented by each point are oriented so as to be exposed to the spray. This is accomplished by defining the segment normal

$$\hat{\boldsymbol{b}}_i = \frac{\overrightarrow{p_{i+1}p_i} \times (0,0,1)}{|\overrightarrow{p_{i+1}p_i} \times (0,0,1)|} \tag{29}$$

and taking the dot product with $\hat{\boldsymbol{n}}$. Thus, the set of points mapped to segment *i* is

$$B_i = \left\{ \boldsymbol{c}_j, \hat{\boldsymbol{n}}_j \,\middle|\, p_{i_\varphi} < c_{j_\varphi} \leq p_{(i+1)_\varphi} \text{ and } \hat{\mathbf{b}}_i \cdot \hat{\boldsymbol{n}}_j > 0 \quad \forall \left(\boldsymbol{c}_j, \hat{\boldsymbol{n}}_j \right) \in C_s \right\} \tag{30}$$

where the subscript φ indicates the angular component of each point's polar coordinate.

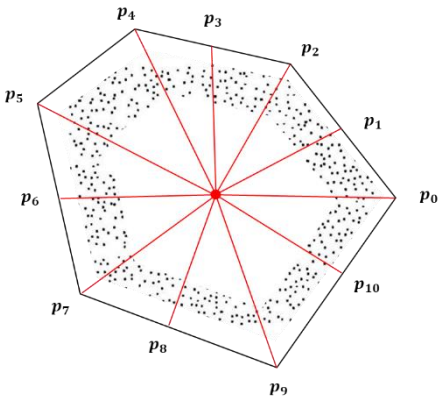

Figure 9: Binning of the Point Cloud to the Convex Hull Path in 2D

Using this collection of binned points, the algorithm has the option to adapt the path by adjusting the distance from the part, the velocity of the move or both for each bin within each slice. The process for using both adaptive methods is relatively straight forward when used separately, the distance-based method looks at the aggregate distance from the end effector to all of the affected points and adjusts accordingly and the time-based method looks at the aggregate incidence angle between the orientation of the end effector and the normal vector of each affected point. However, there is one constraint on how they can be used together. Due to the change in positions created by the distance-based adapting method, which can have an effect on the distance between points and thus the time needed to complete the move, the time-based adapting method must be used after the distance-based method for accurate results.

One of the shortcomings of this methodology is the fact that each adaptive algorithm only considers one data type when making a decision on how to adapt the path. Ideally, every decision should be made with all of the available data, but sometimes different data types can skew the results. In this case, using the incidence angle as an indicator of how much the path offset distance should be adjusted would cause the distance to be adapted too much to the point where the sprayer width is narrower than the offset width. This causes gaps in the raster pattern which then requires replanning later on. Alternatively, using distance from the part to influence the velocity of the end effector does not cause the same path breaking issues, but it doesn't necessarily help all that much either. If the end effector is already too far away, the overall performance of the path would be much better served by adjusting the distance rather than extending the exposure time and thus lengthening the overall execution time.

3.2.6.1.Distance Based Adapting

Given the bins of the path being adapted and the point cloud points that have been matched to each bin, the algorithm defines the distance from each point to the line created by the two end points of the matched bin [40]. Using this distance, the adaptive process can begin by defining the adjustment value for each bin as,

$$\psi_b = \min\left(d_{AG_b} - d_{\mathrm{O}}\,, x d_{\mathrm{O}}\right) \qquad \forall\ b \in B_s \qquad (31)$$

where B_s is the set of all bins on slice *s*, *x* represents the maximum percentage that the path can adapt by with regards to d_{O}, and d_{AG_b} is defined as the aggregate distance value of all points in the bin, which can vary based on the aggregation method. Ideally, this returns a value of zero, meaning no adjustment is needed and the aggregate distance is equal to the desired offset distance. The adjustment value is limited in range so that the path will not be moved within the convex hull by over adjusting. In this case, $x = 0.95$. This is necessary because a value greater than or equal to 1 would result in an adjustment greater than the offset distance itself which would cause the new position to be inside or on the convex hull. While this may not create any collision issues, there is always the possibility and thus is must be accounted for. Alternatively, a minimum distance could be defined and the adjustment would occur on the remaining distance beyond the minimum distance. It should also be noted that the aggregate method used depends on the user's initial input. If necessary, the new path points are determined by,

$$\boldsymbol{p} = \boldsymbol{p} - \left(\widehat{\boldsymbol{n}_p}\,\psi_p\right) \qquad \forall\ \boldsymbol{p} \in P_s \qquad (32)$$

where $\widehat{\boldsymbol{n}_p}$ is the unit vector of the corresponding surface normal, P_s is the path for slice *s*, and ψ_p is the adjustment value of the path point which is defined as,

$$\psi_p = \max\left(\psi_{b_p}, \psi_{b_{p-1}}\right) \tag{33}$$

where ψ_{b_p} is the adjustment value of point *p* in bin *b*. The max of the two bins that share the point is used to ensure that the bin needing the most adjustment gets it. For path smoothness, a moving average of the adjacent bins can be used to determine how much adjustment is needed for each bin by taking the mean of a few adjacent values on both sides of the bin. An example of distance-based adaptation is shown below in Figure 8 as an individual slice of Part C, where both the naïve path, in blue, and the distance adapted path, in orange, have been plotted along with the facets that are captured within the slice, the exact slicing height is shown to the right of the path analysis.

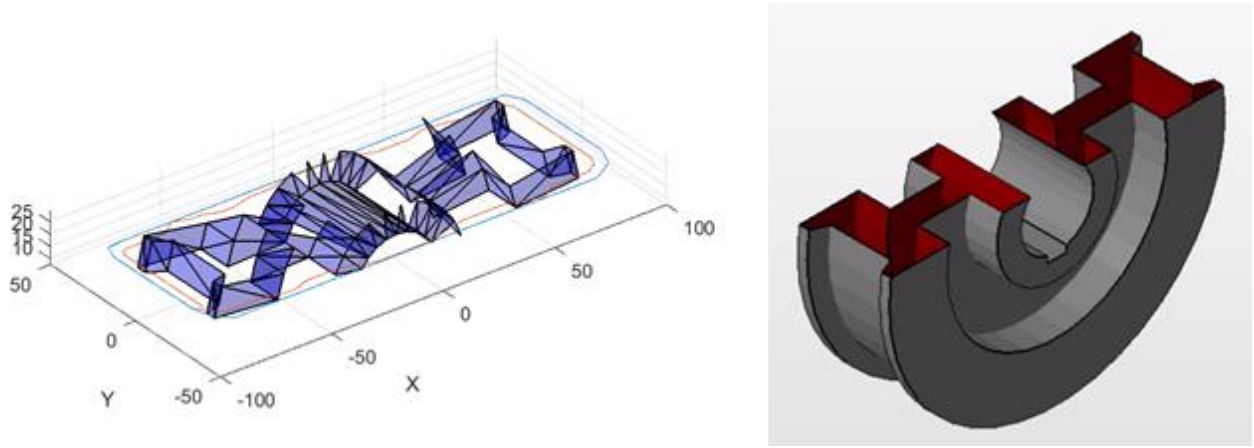

Figure 10: Distance vs Naive Path Plan

3.2.6.2.Time Based Adapting

For this adaptive method, the algorithm determines an incidence value for each point within each bin as illustrated in Figure 9. The incidence value is defined as,

$$\theta_{bc} = (\boldsymbol{n_{b1}} + \boldsymbol{n_{b2}}) \cdot \boldsymbol{n_c} \qquad \begin{matrix} \forall\ b \in B_S \\ \forall\ c \in b \end{matrix} \tag{34}$$

where $\boldsymbol{n}_{b1}$ and $\boldsymbol{n}_{b2}$ are the endpoints of bin *b*, $\boldsymbol{n}_c$ is the normal vector of point *c*, and B_s is the set of all bins on slice *s*. This returns a value between 0 and 1, because any negative values were sorted out earlier when placing points in the bins. When the value approaches 1, that indicates that the angle is very small thus more of the expected amount of effort will be applied to that point.

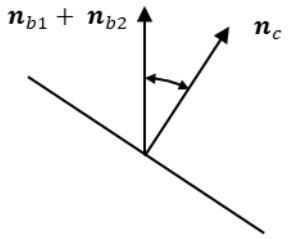

Figure 11: Incidence Angle Calculation

This value is aggregated based on the selected statistical method for bins with multiple points in the same manner as the distance-based method. From these values the speed for each path segment, or bin, is defined as,

$$v_b = v_0\left(x + (1 - x)\,\theta_{AG_b}\right) \qquad \forall\ b \in B_s \qquad (35)$$

where v_0 is the base velocity, B_s is the set of all bins on slice *s*, θ_{AG_b} is the aggregate incidence value of bin *b*, and *x* is an arbitrary value between 0 and 1 that represents a minimum velocity as a percentage of base velocity. In this case, *x = 0.25*, which ensures that the velocity can never be less than 25% of the base velocity and thus the process cannot slow to a complete crawl.

Using this speed, the time between points can be found by,

$$\Delta t_b = d_b / v_b \qquad \forall\ b \in B_s \qquad (36)$$

where Δt_b is the time between the endpoints of bin b, d_b is the distance between the endpoints of bin b, and B_s is the set of all bins on slice *s*. These new time values replace the previously defined values from the original path.

In order to account for the change in speed, an adjusted adaptive value is derived to represent the current amount of work being done during the entire move from one end of the bin to the other. This value is defined as,

$$\tau_{bc} = \theta_{bc} + \left(1 - \frac{v_b}{v_0}\right) \qquad \begin{matrix} \forall\ c\ \in\ C \\ \forall\ b\ \ni\ c \end{matrix} \qquad (37)$$

where θ_{bc} is the incidence angle between point *c* and the end effector moving through bin *b*, which is defined for each bin a point falls in. This results in values that approach 1, the ideal value, but do not achieve 1, unless it was there before and required no adaptation. The closeness to 1 for a given point can be manipulated by changing the value of *x* when determining v_b, where the smaller the value, the closer to 1 these values can become at the expense of time.

3.2.7. Analysis

In order to properly analyze the quality of the path, a single impingement value was assigned to each point in the point cloud derived from the original part that combined measures of both adaptive methods. This impingement value is defined as,

$$\gamma_c = \sum_{\forall\ b\ \ni\ c} \left(\frac{1}{d_{bc}^2}\tau_{bc}\right) \qquad \forall\ c\ \in\ C \qquad (38)$$

where τ_{bc} is the adjusted time-based value for point *c* with regards to bin *b*, d_{bc} is the distance from point *c* to the path of the end effector in bin *b* and $\frac{1}{d_{bc}^2}$ is derived from the well-known Inverse

Square Law. The summation across all bins *b* that contain point *c* accounts for any overlap between slices that may cause a point to be captured twice and thus receive more work overall.

3.2.8. Experimental Design

In order to determine the best method for producing better toolpaths, two factors were considered. The type of adaptive algorithm used, which has two levels: Distance and Distance + Time, and the type of statistical aggregate method used, which has four levels: Mean, Mode, Min and Max. These factors, along with a Naïve path, with no adaptive adjustments, combine to create nine different treatments. Aside from the usual summary statistics, a bin metric was developed to better measure the distribution of total cleaning applied across the entire part and is defined as,

$$\zeta = \sum_{c=0}^{\eta} \sum_{j=1}^{\beta} \begin{cases} b_{\min} \leq \gamma_c < b_{\max}, & j \\ else, & 0 \end{cases} / \eta \tag{39}$$

where η is the number of facets on the part, γ_c is the impingement value of facet *c*, β is the number of bins, *j* is the bin iterator, and $b_{\min}$ and $b_{\max}$ are the endpoints of each bin that are defined as,

$$b_{\min} = \gamma_{\min} + (j-1)\frac{\gamma_{\max} - \gamma_{\min}}{\beta} \qquad b_{\max} = \gamma_{\min} + j\frac{\gamma_{\max} - \gamma_{\min}}{\beta} \tag{40}$$

where $\gamma_{\min}$ is the minimum impingement value and $\gamma_{\max}$ is the maximum impingement value of all parts being compared. This yields a result between one and the number of bins, with higher values indicating a better overall toolpath. The total time and distance needed to complete the toolpath were also considered to see what kind of trade-off occurs when the path is adapted.

A set of five test parts were chosen to be used in this analysis as shown in Figure 10. Two of the parts, A and B, were specifically designed to demonstrate how the planner makes adjustments to the path, while the other three were taken from online 3D CAD databases to represent common geometries encountered in the real world. Each of the parts were sliced using the exact same

parameters and were positioned as demonstrated in Appendix A. These parameters are: offset distance, d_O = 11 units; sprayer angle, $\theta = 60°$; base velocity, v = 10 units/second; overlap percentage, σ = 10 %. The slices themselves were considered as parallel XY planes with a varying Z axis value. The downside to slicing in one direction is that any facets on the "top" or "bottom" of the part will most likely not get covered. The easiest solution would be to slice the part in two different directions to ensure total coverage. In this research, only one slicing direction is considered due to computationally efficiency and to be more consistent when comparing across parts.

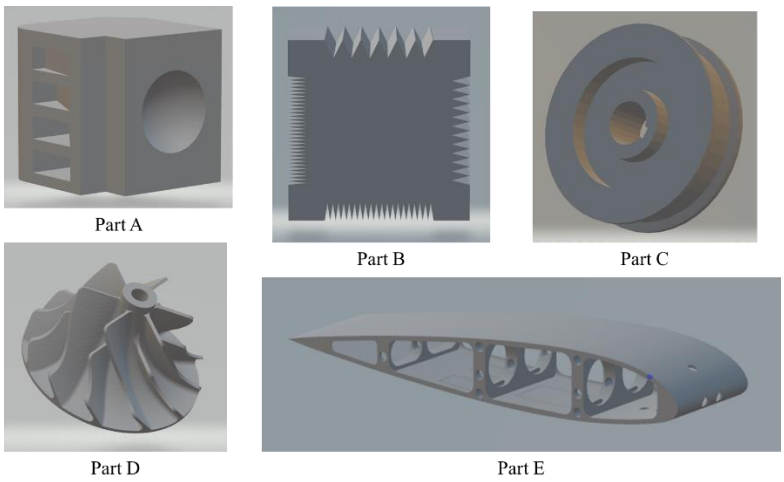

Figure 12: Test Parts Used for Analysis

3.3. RESULTS

These results come from a set of five test parts that are shown in Appendix A. Two of the parts were specifically designed to demonstrate how the planner makes adjustments to the path, while the other three were taken from online 3D CAD databases to represent common geometries encountered in the real world. Preliminary analysis was performed via ANOVA analysis to test for interactions between the two factors. A two-way analysis considered the statistical method to

be multi-colinear and threw it out. Upon further analysis, a one-way ANOVA analysis showed that there was some significance to the type of statistical method used, which is expected as the aggregation method directly effects all values in the same and generally equal manner. In other words, common sense would indicate that adaptation based off of the minimum values would be greater than for the mean, which would be greater than if the max was used. Going forward this analysis will focus on the difference between adaptive methods by averaging the values from each treatment grouped by adaptive method. The aggregate results of all parts are shown in Table 1.

Table 1: Average Adaptive Method Results

Adaptive Algorithm	Mean Impingement	Bin Metric	Total Path Time	Total Path Length
Distance	0.00270	1.264	318.856	3215.599
Distance + Time	0.00390	1.474	513.151	3215.599
Naïve	0.00177	1.131	309.094	3117.976

Along with the data above, both a histogram and a kernel density estimate (KDE) of the probability density function were created for each treatment of each part. For clarity, the KDE's have been trimmed to show only positive values up to the 95^{th} percentile. This is done because these estimates do not take into account that the values cannot be negative and the extreme values can cause the data to be very hard to read. The histograms have also been trimmed to zoom in on the densest areas of the distribution to better observe the change between each treatment. In this case, the histogram zooms in on the range 0 - 0.01, and all values greater than 0.01 are contained in their own bin. Along with these comparisons between each treatment as a function of impingement, the tradeoffs with making the adaptations were also considered. The resulting values were plotted against the total time taken to complete the path in both actual values and percent difference from the naïve path. Figure 11 contains the KDE's for adaptive algorithm and

aggregation method as well as a plot of each treatments bin metric vs time in columns 1-3 respectively, and each row A-E references the corresponding part. Individual part results and heat maps are also included in the text below. In the heatmaps, red indicates more cleaning and blue indicates less or none at all. All other figures and results are contained in the appendices. Appendix A contains the original parts, Appendix B contains the KDE's, Appendix C contains the histograms, Appendix D contains the trade-off plots, Appendix E contains the individual treatment results for each part, and Appendix F contains a nomenclature table for all equations.

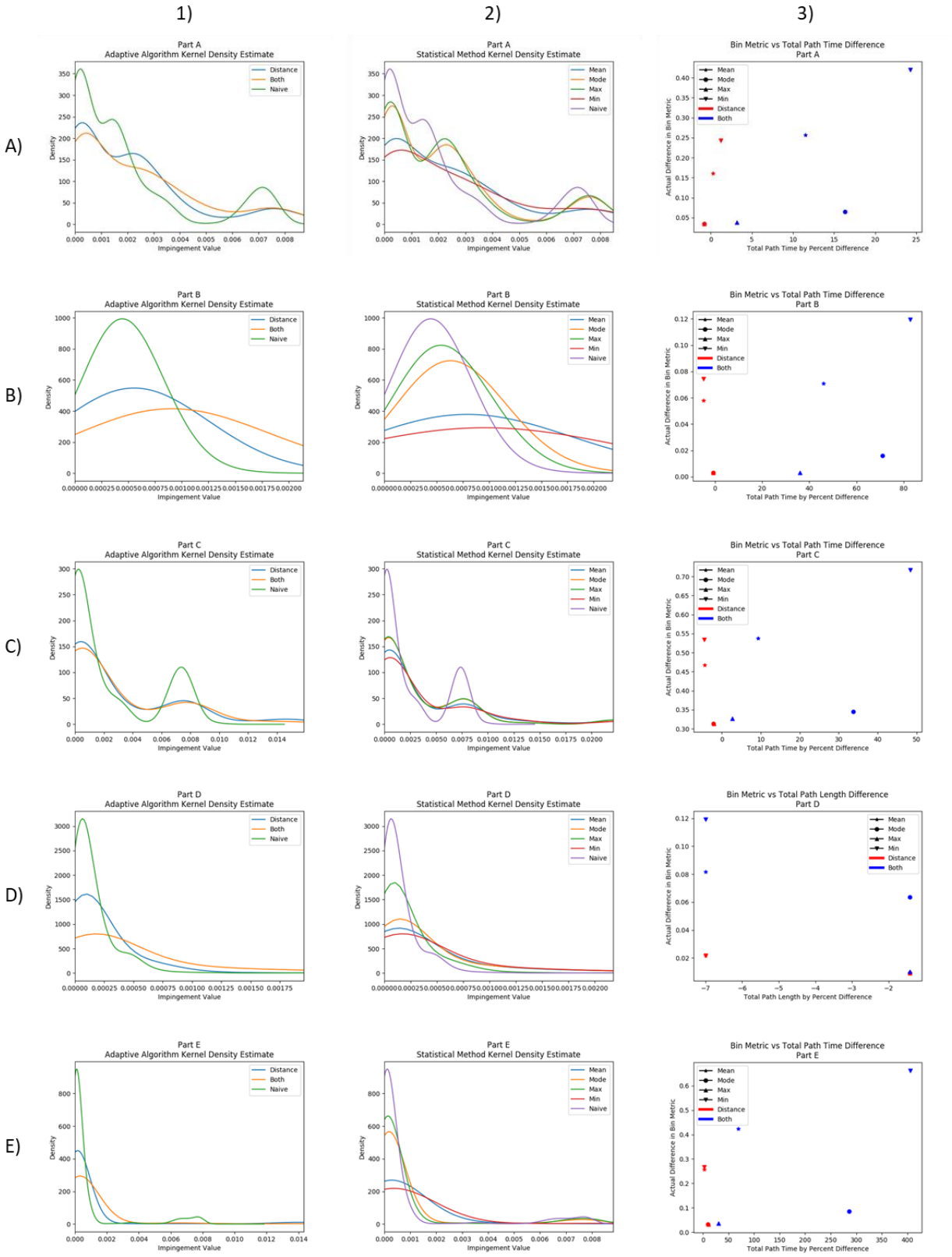

Figure 13: Summary Plots for All Parts and Treatments

Part A is a specifically designed test cube intended to show how the algorithm reacts to concavities and other changes in geometry. Each side and corner are designed to test a different geometric form. Shown here in Figure 12 is a concave half sphere at each level of cleaning. Here the blue center indicates areas beyond the effective reach of the sprayer. This area lessens when distance adaptation is used, but remains roughly the same when time is added, although the colors around it shift closer to red. This can also be seen in Figure 11(A1) where there is a spike in higher values as time is added on to the distance adapted path. This results in an improvement of the bin metric by ~0.1 at the cost of an ~10% increase in time to execute shown in Figure 11(A3).

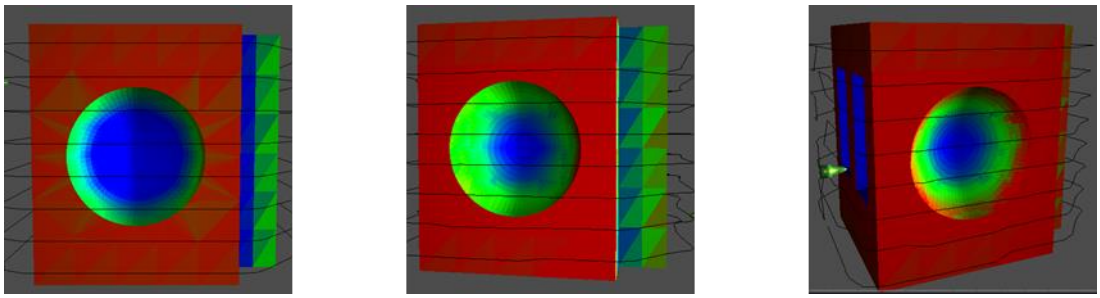

Figure 14: Part A Heatmap at Each Adaptive Algorithm Level (Naïve, Distance, Distance+Time)

Part B a specifically designed test cube intended to show how the algorithm reacts to changes in incidence angle and thus how it adapts velocity and time. While the results are a bit difficult to see as the mean surface is mostly convex and requires little path variation, when viewed in real time, a real change in velocity can be observed. This part also demonstrates one of the key issues with flat surfaces on the convex hull. There is a distinct difference of coloration between facets on the same plane due to the large facet size which causes the centroids to be captured in different slices and thus adapted differently. Figure 17(a) demonstrates this issue for a single slice. This also causes the path to be unevenly adapted despite the mean surface being consistent

throughout. Here, the bin metric only improves by ~0.02 at the cost of nearly a ~40% increase in total path time shown in Figure 11(B3).

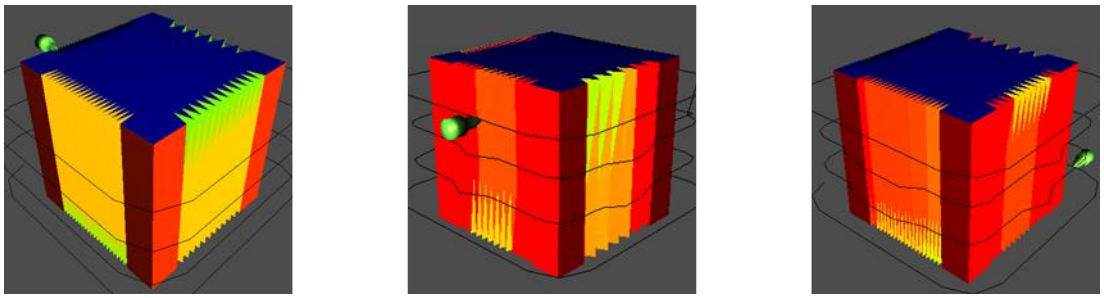

Figure 15: Part B Heatmap at Each Adaptive Algorithm Level (Naïve, Distance, Distance+Time)

Part C is a simplified wheel rim that has been sliced in the vertical orientation to provide more complexity as opposed to being sliced laying down. One of the unique features of this part is that, due to the edge of the rim, the bins on the path tend to catch points with very different normal vectors and distances. This part experiences some inconsistent impingements due to the sampling error described above. The interior of the wheel also showcases facets within the effective spraying distance, but with perpendicular normal that receive almost no significant cleaning as well as facets that have completely parallel surface normal but still can't meet the minimum effective spray distance despite distance adaptation. This is apparent through the distinct peaks shown in Figure 11(C1-2). This part experiences a similar trade-off as part A, where an ~0.1 increase in the bin metric is seen at the cost of an ~10% increase in total path execution time.

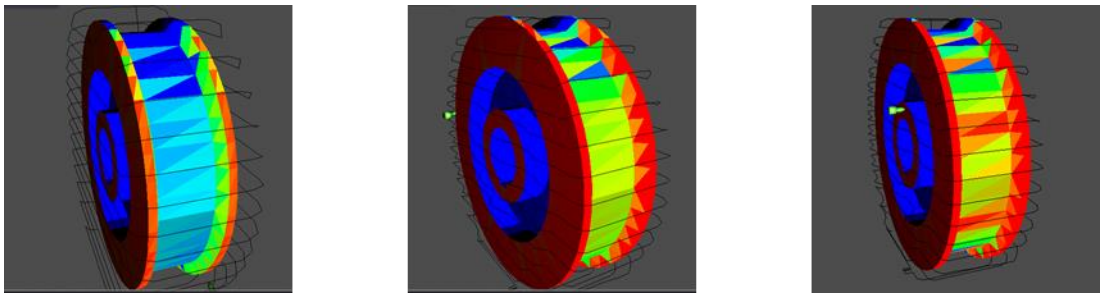

Figure 16: Part C Heatmap at Each Adaptive Algorithm Level

(Naïve, Distance, Distance+Time)

Part D is a rotor blade from an engine that has been reduced from its original facet count for computational efficiency. The original part is shown in Appendix A. While this may look ugly, it is a good approximation of the surface for the algorithm's purposes and allows for each facet to be considered and given an impingement value, which is very difficult to do when the part is down sampled. Due to the shape of the rotor, distance-based adaptation for the full part is hindered by the edges of each fin, as shown in Figure 17(b). However, it is still very effective compared to the naïve path. This hinderance allows the time-based method to be more effective than usual as it cuts the peak of lower values in half from the distance only method as shown in Figure 11(D1), which is not seen in any of the previous parts tested. However, this still only represents an ~0.06 increase in the bin metric while nearly doubling the completion time from the mean values. If the minimum is used, an ~0.12 increase can be achieved, but it takes nearly 5 times as long to complete as shown in Figure 11(D3).

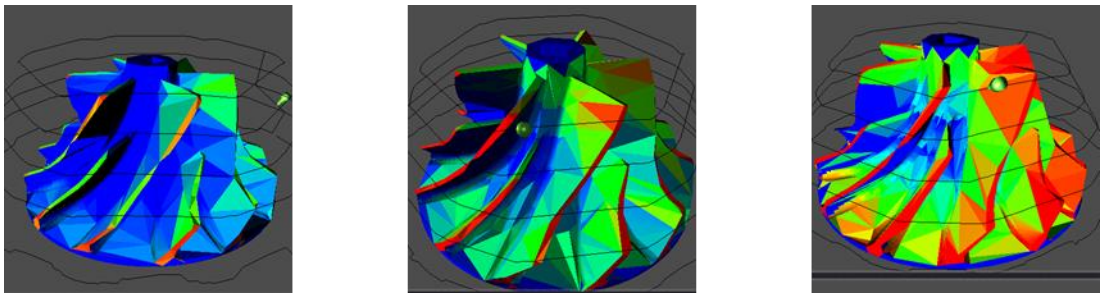

Figure 17: Part D Heatmap at Each Adaptive Algorithm Level

(Naïve, Distance, Distance+Time)

Part E is a cross section of an airplane wing that has also been reduced to facilitate computational speed. Here the reduction does not have a large effect on the visible geometry. This part represents an extreme challenge of tool point accessibility. In this case, the sprayer cannot invade the convex hull, which makes it very hard to effectively cover a large portion of the part. This can be seen in the relatively small change in the distribution in Figure 11(E1) as well as in the individual slice path in Figure 17(c). Here, the naïve path's peak at higher impingement values is smoothed out across the higher values and appears to disappear while the lower values are slightly reduced and shifted only by a very little bit. This is a part, that while easily planned for externally, the interior will continue to remain a challenge until effective accessibility algorithms are included in the path planning. This difficulty in accessing the interior is seen most sharply in the difference between the distance and distance + time bin metrics. Here there is an increase of ~0.15, the highest of all the tested parts, at a cost of only a ~50% increase in execution time., which is much better than the ~500% needed to achieve a worse result in part D.

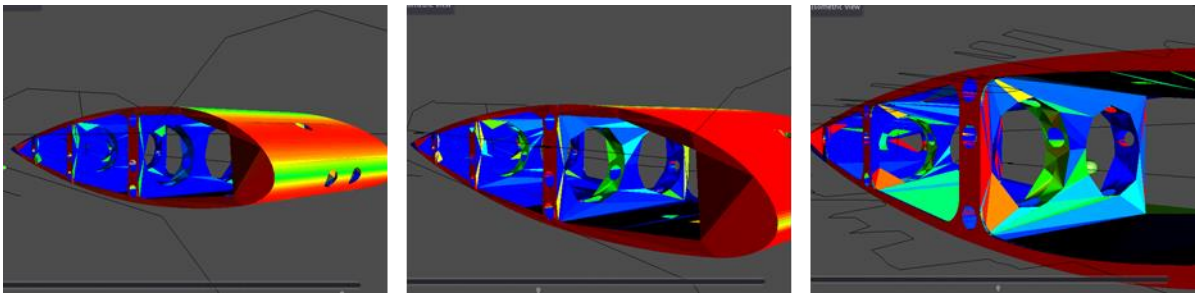

Figure 18: Part E Heatmap at Each Adaptive Algorithm Level

(Naïve, Distance, Distance+Time)

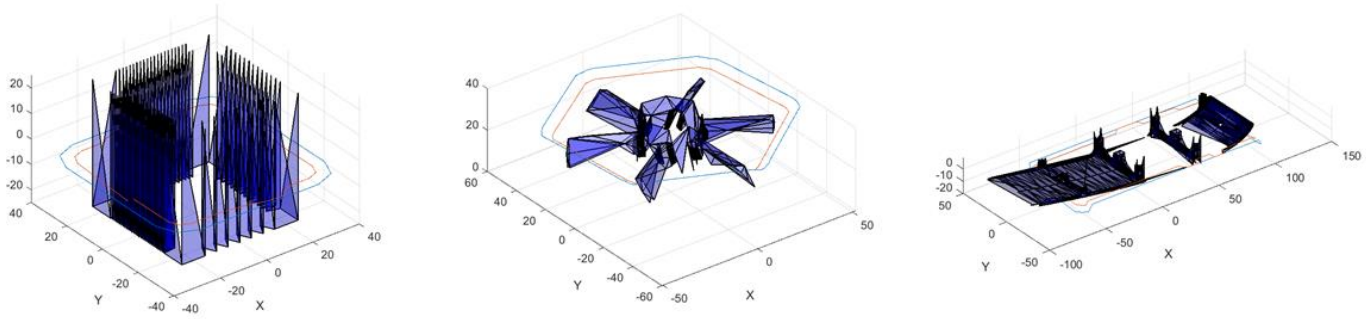

Figure 19: Naive vs Distance Adapted Paths; (a) Part B (left), (b) Part D, (c) Part E (right)

3.4. DISCUSSION

From these results, the most consistent, effective and cheapest, in terms of computation time, method for adapting the naïve path is as follows: Begin by adapting the naïve path using the distance-based method, evaluate the quality of the path and if a standard is not met, adapt the path based on time if required. Otherwise, the time-based adaptive method is not needed. This can be seen across all of the adaptive algorithm charts in column 1 of Figure 11 which shows a significant decrease in low impingement values from the naïve to the distance adapted path and again when adapting by both distance and time and is summarized in Figure 18. While the values in the figure for parts B and D are not exactly convincing, they can be explained by geometric abnormalities as discussed above. Overall, these findings are consistent with the fact that work done by spraying is

highly nonlinear when adjusting distance, which makes it a critical part of the process when calculating actual work done. This method was also chosen because the benefits of adapting based on time are nowhere close to the benefits of adapting by distance and choosing only to use it if the distance method cannot meet the requirements saves significant computational time. Aside from computational time, adjusting the time for each bin generally creates a longer path completion time, which is not ideal. Further compounding the issue of time, some distance adjustments can actually lessen the overall completion time. It should also be noted that the mean aggregation method is preferred because it gives a better representation of all points in a bin. While taking the minimum definitely returns better values, it can be unnecessarily affected by outliers. The same holds true for the maximum value. And while the mode might make sense, these are continuous values and thus it is not very likely to consistently find multiple occurrences of the same value. The difference between using max and min values can also be made up by increasing the sprayer pressure.

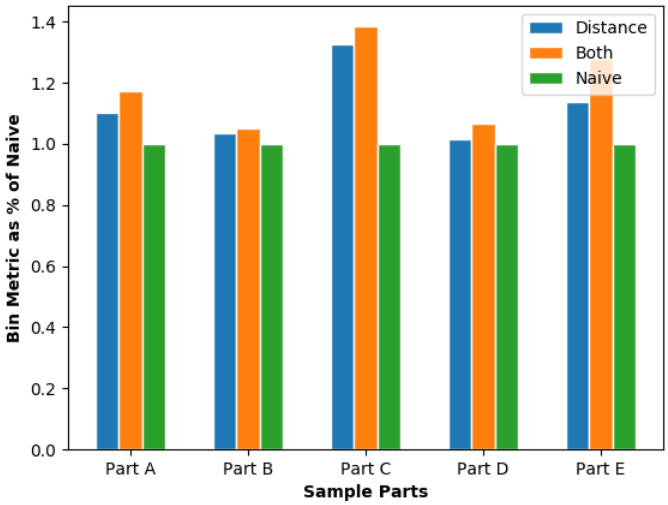

Figure 20: Bin Metric Comparison Across All Parts

At the beginning, the rationale for developing this algorithm was to allow for smooth path planning for very complex parts, which is something it excels at. No matter what geometry is provided to the planner, the resulting path will always resemble a convex part with accessible tool points barring any robot specific accessibility issues. Other than reach, there are no geometrical constraints preventing the execution of the resulting path. For the largest parts, placing them on a rotary table would allow for a robot with a smaller accessible workspace to fully execute the path. While this path will certainly cover the part, the adaptive methods used allow for more contextualized paths that would not be possible with a simple slicing method on the convex hull. The natural alternative to this would be to forgo any convex hull path and then slice the part itself directly. However, the idiosyncrasies of the resulting path would more than likely be very difficult for a robot to achieve in a smooth fashion.

This adapted path is especially useful in situations where quality path plans are needed in a timely manner that do not require perfect precision, without any or minimal human interaction. As mentioned previously, one-off path planning is a good application for this methodology, along with being used as a starting point for mass produced toolpaths that can be tweaked by a human operator. While these adapted paths do a good job of accommodating the surface topology of the original part despite being built from the convex hull, the paths could be improved by defining a safe way to invade the convex hull without creating any collision issues. There are a variety of tool accessibility and visibility algorithms available to verify whether or not a defined path is achievable or not [41]. However, the computational load required for these methods would significantly slow down the path building process. With that being said, it is certainly possible to improve computational time by reworking the algorithms and using better processors to a point where this difference is negligible.

As discussed previously, there are some shortcomings to this methodology. Ideally, every decision should be made with as much relevant data as possible, but sometimes different data types can skew the results. In this case, using the incidence angle as an indicator of how much the path offset distance should be adjusted would cause the distance to be adapted too much to the point where the sprayer width is narrower than the offset width. This causes gaps in the raster pattern which then requires replanning later on. Alternatively, using distance from the part to influence the velocity of the end effector does not cause the same path breaking issues, but it doesn't necessarily help all that much either. If the end effector is already too far away, the overall performance of the path would be much better served by adjusting the distance rather than extending the exposure time and thus lengthening the overall execution time.

Another drawback to slicing based methods is that there are usually two sides left uncovered. When sliced along the Z axis, the top and bottom sides are the ones left uncovered. For complete coverage, the part can be sliced along a different axis to cover the uncovered sides. Currently, the slicing direction is determined from user input and is derived as being perpendicular to one of the three axes. For more accurate slicing, the slicing planes could be derived as being perpendicular to any arbitrary vector and methods could be developed for defining that vector based on the overall orientation of all of the facets. Theoretically, the ideal slicing direction would be perpendicular to the average normal vector of all facets, but the specifics require a more thorough investigation.

As more and more complex path planners are developed, the benefit of saving time by only adapting the distance may fade depending on the process parameters. When the distance is shortened too much and the overlap percentage is not large enough to compensate, there is the possibility of gaps being left in between passes of the sprayer as described above. In order to ensure

complete coverage, the adjusted section would need to be replanned with a thinner slice thickness, which would result in multiple passes and ultimately more time used. Currently, this replanning is achieved through a separate process that requires user feedback, but in the future a dynamic system that can achieve this on the fly is ideal. Regardless, these path plans provide a good starting point for human iteration by identifying the areas on the part that need more cleaning, whether this be in a collaborative system or as the beginning of a path plan for a mass-produced part. Eventually, these systems will get to the point where they can effectively cover any part placed within their reachable volume on their own with no human intervention required.

3.5. CONCLUSIONS

As robots continue to ingrain themselves within industrial settings, it is only a matter of time until fully autonomous systems are the norm. This two-pronged approach to generalized path planning, planning for the convex hull and then adjusting for the original part, removes a lot of the difficult geometrical problems from the equation. When comparing adaptive methods and considering tradeoffs for the simplified paths, it is clear that adjusting based on distance is the most effective way of achieving better results, although using both methods does produce better toolpaths and can be justified depending on the trade-off with time on that part. If nothing else, these results indicate that it is possible to achieve good toolpaths without intricate and time-consuming path planning algorithms by sacrificing some precision. Moving forward, there are plenty of improvements that can be made, in any number of areas, but this algorithm does provide a good stepping off point for agile path planning for industrial spraying operations of novel complex parts.

3.6. REFERENCES

[1] A. Woods and H. Pierson, "Developing an Ergonomic Model and Automation Justification for Spraying Operations," in *Institute of Industrial and Systems Engineers Annual Conference*, Orlando, FL, 2018.

[2] H. Chen, T. Fuhlbrigge and X. Li, "Automated Industrial Robot Path Planning for Spray Painting," in *4th IEEE Conference on Automation Science and Engineering*, Washington, D.C., 2008.

[3] J. S. Oh, Y. H. Choi, J. B. Park and Y. F. Zheng, "Complete Coverage Navigation of Cleaning Robots Using Triangular-Cell-Based Map," *IEEE TRANSACTIONS ON INDUSTRIAL ELECTRONICS*, vol. 51, pp. 718-726, 2004.

[4] Z. He, B. Lu, J. Hong, Y. Wang and Y. Tang, "A novel arc-spraying robot for rapid tooling," *International Journal of Advanced Manufacturing Technologies*, 2007.

[5] W. Chen and D. Zhao, "Path Planning for Spray Painting Robot of Workpiece Surfaces," *Mathematical Problems in Engineering*, 2013.

[6] W. Sheng, N. Xi, M. Song, Y. Chen and P. Macneille, "Automated CAD-guided robot path planning for spray painting of compound surfaces," in *IEEE/RSJ International Conference on Intelligent Robots and Systems*, Takamatsu, Japan, 2000.

[7] A. M. Kabir, J. D. Langsfeld, S. Shriyam, V. S. Rachakonda, C. Zhuang, K. N. Kaipa, J. Marvel and S. K. Gupta, "Planning Algorithms for Multi-Setup Multi-Pass Robotic Cleaning with Oscillatory Moving Tools," in *IEEE International Conference on Automation Science and Engineering (CASE)*, Fort Worth, TX, 2016.

[8] Y.-H. Choi, T.-K. Lee, S.-H. Baek and S.-Y. Oh, "Online Complete Coverage Path Planning for Mobile Robots Based on Linked Spiral Paths Using Constrained Inverse Distance Transform," in *The IEEE/RSJ International Conference on Intelligent Robots and Systems* , St. Louis, MO, 2009.

[9] E. Galceran and M. Carreras, "A survey on coverage path planning for robotics," *Rovotics and Autonomous Systems*, vol. 61, pp. 1258-1276, 2013.

[10] C. Luo, S. X. Yang, D. A. Stacey and J. C. Jofriet, "A Solution to Vicinity Problem of Obstacles in Complete Coverage Path Planning," in *IEEE International Conference on Robotics 8 Automation*, Washington DC, 2002.

[11] J. H. Lee, J. S. Choi, B. H. Lee and K. W. Lee, "Complete Coverage Path Planning for Cleaning Task using Multiple Robots," in *IEEE International Conference on Systems, Man, and Cybernetics*, San Antonio, TX, 2009.

[12] S. X. Yang and C. Luo, "A Neural Network Approach to Complete Path Planning," *IEEE TRANSACTIONS ON SYSTEMS, MAN, AND CYBERNETICS—PART B: CYBERNETICS,* vol. 34, pp. 718-724, 2004.

[13] A. UGUR, "Path planning on a cuboid using genetic algorithms," *Information Sciences,* vol. 178, pp. 3275-3287, 2007.

[14] J. C. Rubio, J. Vagners and R. Rysdyk, "Adaptive Path Planning for Autonomous UAV Oceanic Search Missions," in *AIAA 1st Intelligent Systems Technical Conference,* Chicago, IL, 2004.

[15] F. Schwarzer, M. Saha and J.-C. Latombe, "Adaptive dynamic collision checking for single and multiple articulated robots in complex environments," *IEEE Transactions on Robotics,* vol. 21, no. 3, pp. 338-353, 2005.

[16] R. Bohlin and L. Kavraki, "Path planning using lazy PRM," in *IEEE International Conference on Robotics and Automation,* San Francisco, CA, 2000.

[17] A. Pichler, M. Vincze, K. Hausler, H. Andersen and O. Madsen, "A Method for Automatic Spray Paiiitiiig of Uiiknowii Parts," in *IEEE International Conference on Robotics & Automation,* Washington DC, 2002.

[18] E. U. Acar, H. Choset, Y. Zhang and M. Schervish, "Path Planning for Robotic Demining: Robust Sensor-based Coverage of Unstructured Environments and Probabilistic Methods," *The International Journal of Robotics Research* , vol. 22, pp. 441-466, 2003.

[19] M. Hebert and E. Krotkov, "3-D Measurements From Imaging Laser Radars: How Good Are They?," in *International Workshop on Intelligent Robots and Systems* , Osaka Japan, 1991.

[20] F. Remondino and S. El-Hakim, "IMAGE-BASED 3D MODELLING: A REVIEW," *The Photogrammetric Record,* vol. 21, pp. 269-291, 2006.

[21] F. Blais, "Review of 20 years of range sensor development," *Journal of Electronic Imaging,* vol. 13, pp. 231-240, 2004.

[22] D. K. Pai, K. v. d. Doel, D. L. James, J. Lang, J. E. Lloyd, J. L. Richmond and S. H. Yau, "Scanning Physical Interaction Behavior of 3D Objects," in *SIGGRAPH*, Los Angeles, CA, 2001.

[23] M. Levoy, K. Pulli, B. Curless, S. Rusinkiewicz, D. Koller, L. Pereira, M. Ginzton, S. Anderson, J. Davis, J. Ginsberg, J. Shade and D. Fulk, "The Digital Michelangelo Project: 3D Scanning of Large Statues," in *SIGGRAPH*, New Orleans, LA, 2000.

[24] C.-F. Huang, Y.-C. Tseng and L.-C. Lo, "The Coverage Problem in Three-Dimensional Wireless Sensor Networks," in *IEEE Globecom*, Dallas, 2004.

[25] J. D. Schutter, T. D. Laet, J. Rutgeerts, W. Decré, R. Smits, E. Aertbeliën, K. Claes and H. Bruyninckx, "Constraint-based Task Specification and Estimation for Sensor-Based Robot Systems in the Presence of Geometric Uncertainty," *The International Journal of Robotics Research*, vol. 26, pp. 433-455, 2007.

[26] J. Tegin and J. Wikander, "Tactile sensing in intelligent robotic manipulation – a review," *Industrial Robot: An International Journal* , pp. 64-70, 2005.

[27] P. Meng, E. S. Geskin, M. C. Leu, F. Li and L. Tismeneskiy, "An Analytical and Experimental Study of Cleaning With Moving Waterjets," *J. Manuf. Sci. Eng.*, vol. 120, no. 3, pp. 580-589, 1998.

[28] S.-H. Suh, I.-K. Woo and S.-K. Noh, "Development of An Automatic Trajectory Planning System (ATPs) for Spray Painting Robots," in *Intemational Conference on Robotics and Automation*, Sacremento, CA, 1991.

[29] H. Chen, W. Sheng, N. Xi, M. Song and Y. Chen, "Automated Robot Trajectory Planning for Spray Painting of Free-Form Surfaces in Automotive Manufacturing," in *IEEE International Conference on Robotics 8 Automation*, Washington DC, 2002.

[30] A. Djuric, R. J. Urbanic and J. L. Rickli, "A Framework for Collaborative Robot (CoBot) Integration in Advanced Manufacturing Systems".

[31] *ISO/TS 15066:2016 Robots and robotic devices -- Collaborative robots*, International Organization for Standardization, 2016.

[32] P. Waurzyniak, "Putting Safety First in Robotic Automation," *Manufacturing Engineering*, pp. 61-66, September 2016.

[33] T. Anandan, "Robotic Industry Insights: Collaborative Robots and Safety," Robotic Inustries Association, 26 Jan 2016. [Online]. Available: https://www.robotics.org/content-detail.cfm?content_id=5908.

[34] Universal Robots, "Afraid to Commit? No Problem, with Flexible, Redeployable Cobots," 3 June 2016. [Online]. Available: https://blog.universal-robots.com/flexible-redeployable-cobots. [Accessed 30 April 2017].

[35] Robotiq, "Teaching Robots Welding," [Online]. Available: http://robotiq.com/solutions/robot-teaching/. [Accessed 6 May 2017].

[36] P. Stone and M. Veloso, "Towards collaborative and adversarial learning: a case study in robotic soccer," *International Journal of Human-Computer Studies,* vol. 48, pp. 83-104, 1998.

[37] R. Mitnik, M. Recabarren, M. Nussbaum and A. Soto, "Collaborative robotic instruction: A graph teaching experience," *Computers and Education,* vol. 53, pp. 330-342, 2009.

[38] S. Brown and H. Pierson, "A Collaborative Framework for Robotic Task Specification," *Procedia Manufacturing,* vol. 17, pp. 270-277, 2018.

[39] C. Connolly, "Cumulative generation of octree models from range data," in *IEEE International Conference*, 1984.

[40] Roman, "Find the shortest distance between a point and line segments (not line)," August 2017. [Online]. Available: https://stackoverflow.com/questions/27161533/find-the-shortest-distance-between-a-point-and-line-segments-not-line.

[41] D. Dakdouk, "Tool Accessibility with Path and Motion Planning for Robotic Drilling and Riveting," Ryerson University, 2016.

[42] D. Vinayagamoorthy, "Rotor Blade," 29 Ocotober 2017. [Online]. Available: https://grabcad.com/library/rotor-blade-8.

[43] C. Domingos, "Wing_Section_NACA23015C200," 2 January 2018. [Online]. Available: https://grabcad.com/library/wing_section_naca23015c200-1.

[44] F. H. Macias, "rueda motriz e inducida grua viajera," 21 September 2017. [Online]. Available: https://grabcad.com/library/rueda-motriz-e-inducida-grua-viajera-1.

3.7. APPENDIX A – Test Parts

3.7.1. Part A - Test Part

A test part designed to test both distance and time based methods using simple geometrical structures. Shown here in a slightly angled view for visibility, otherwise it was sliced as is.

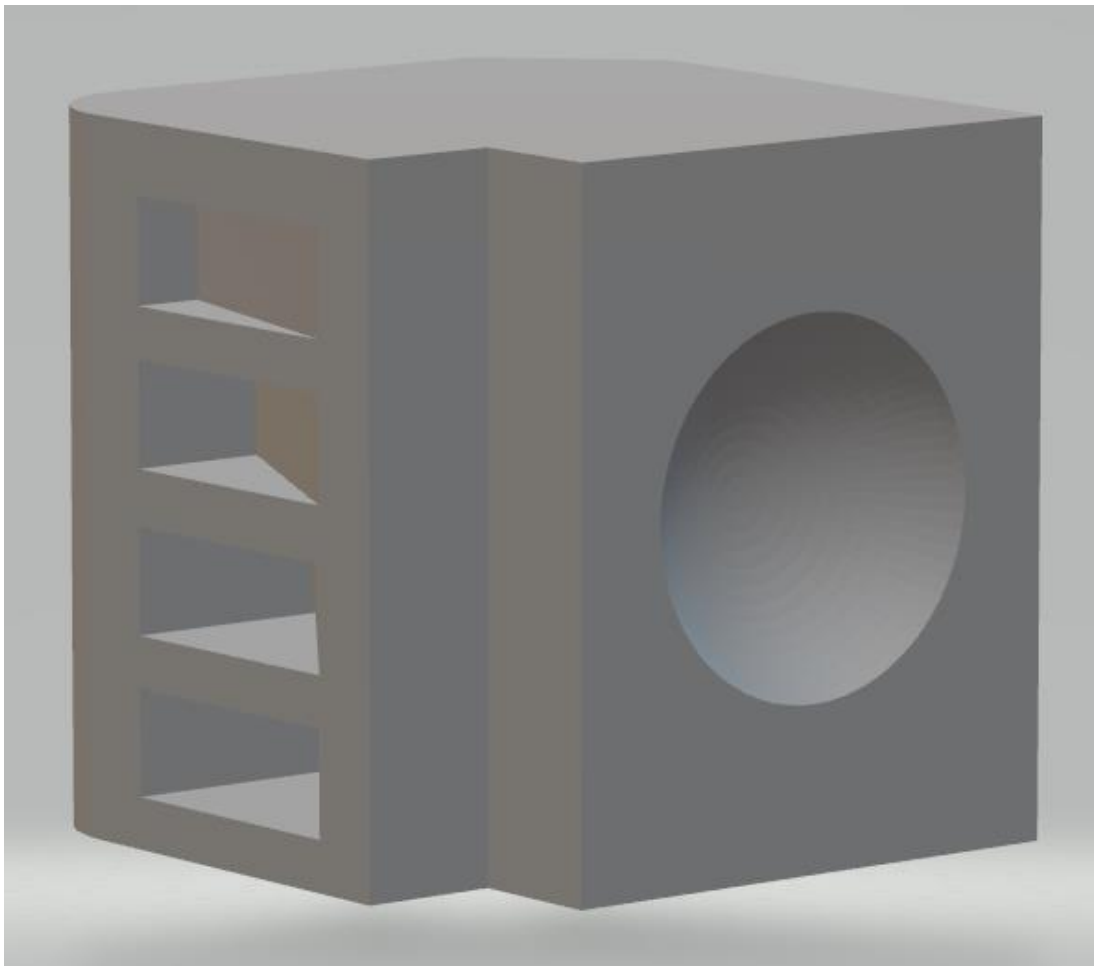

3.7.2. Part B - Incidence Test

A test part designed to isolate the time adaptive method by varying the angle of incidence on each side of the cube. It is shown here in a top down view. The slicing occurred with the piece in its regular orientation.

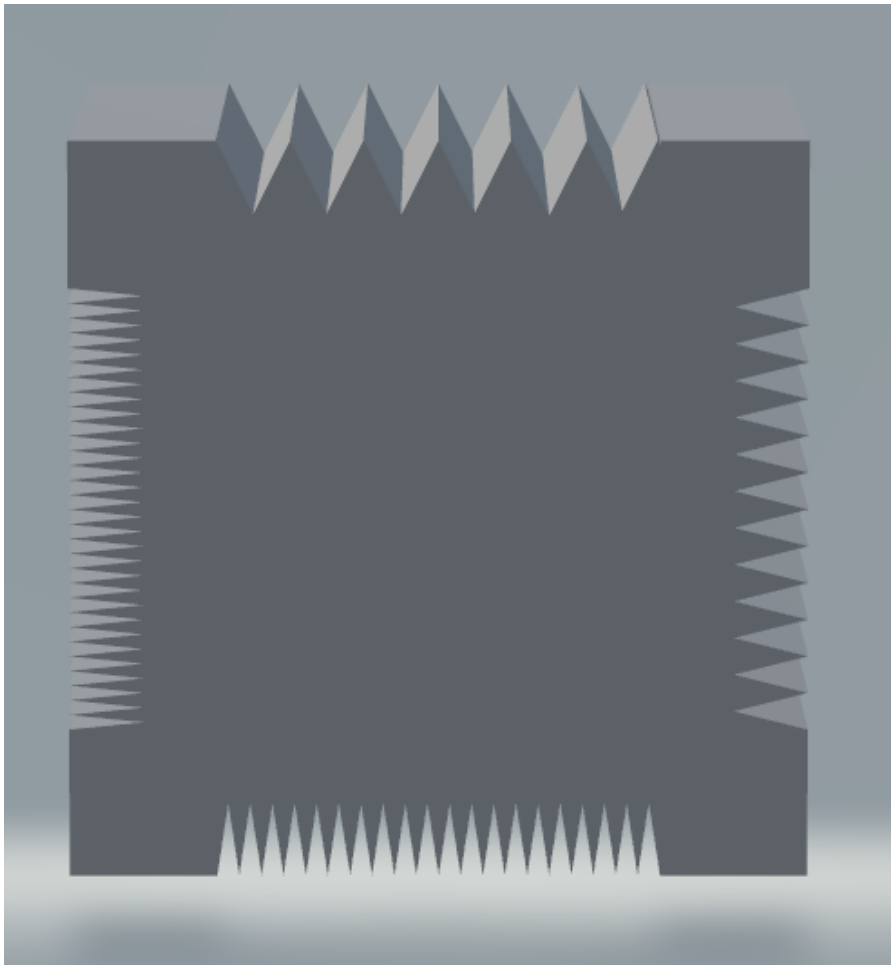

3.7.3. Part C - Solid Wheel Upright

A simplified version of a wheel with minimal internal geometry [44]. Shown here in a slightly angled view for visibility. It was sliced in the vertical orientation as it would appear on a car's axle.

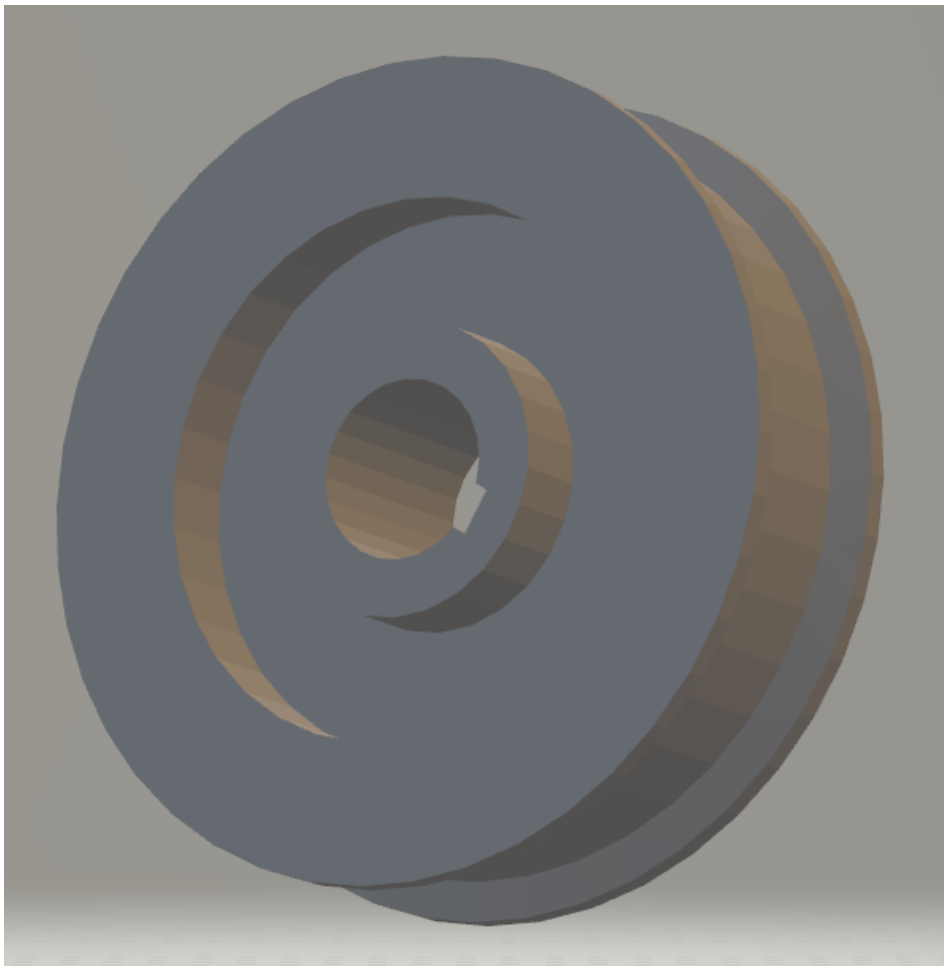

3.7.4. Part D - Blade Reduced

A rotor blade found in an engine [42]. The part has been angled for visibility, but it was sliced with the wide circle as the base with the visible hole facing upwards.

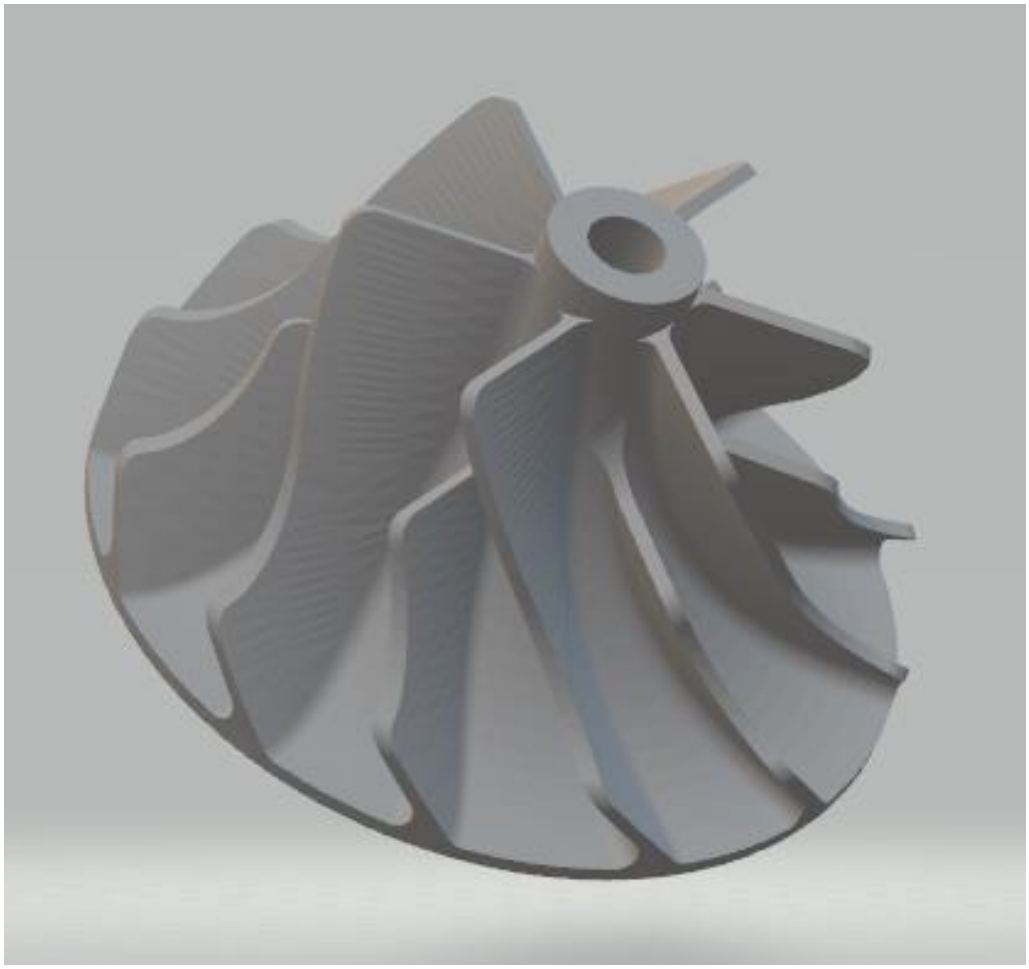

3.7.5. Part E - Wing Section Reduced

A cross section of an airplane wing [43]. Shown here in a slightly angled view for visibility, otherwise it is sliced as is.

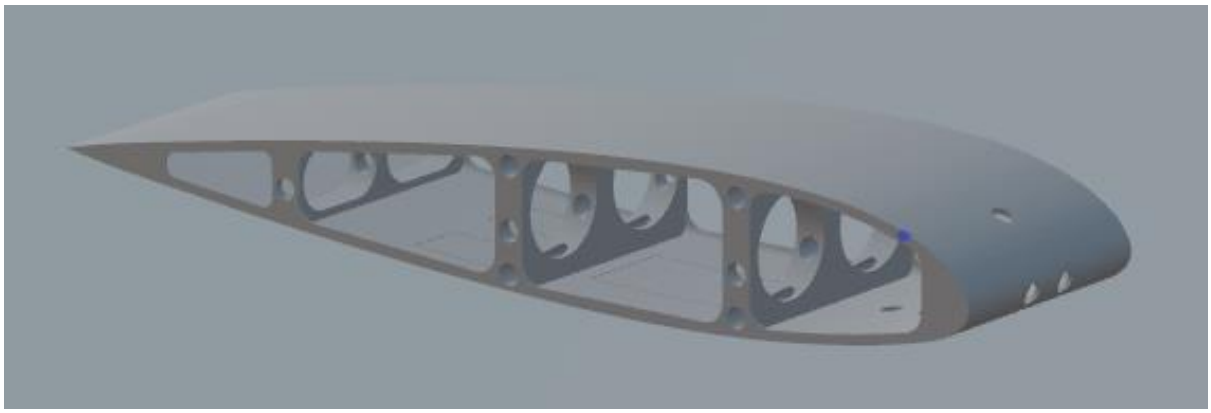

3.8. APPENDIX B – Kernel Density Estimates

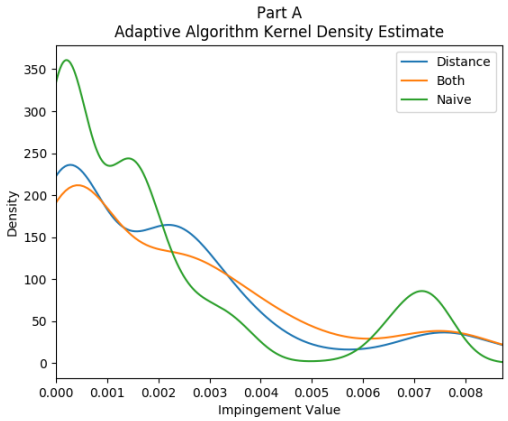

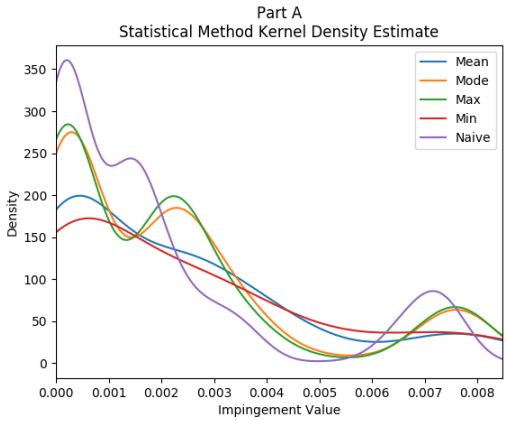

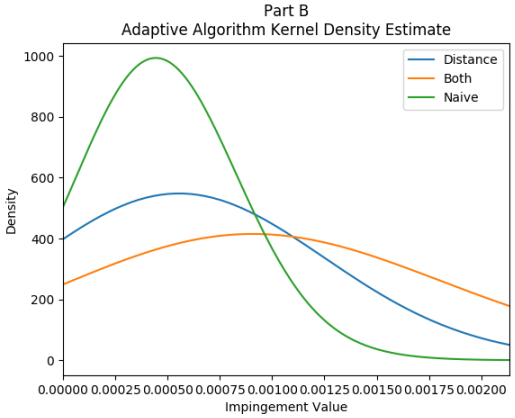

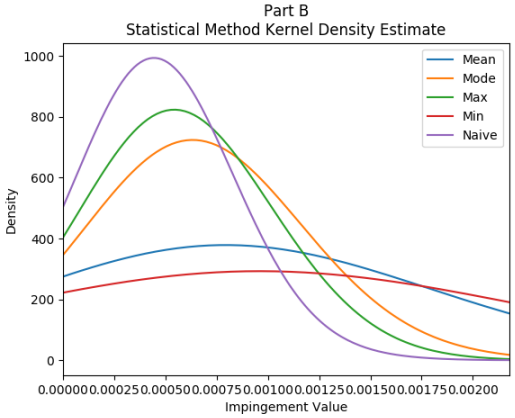

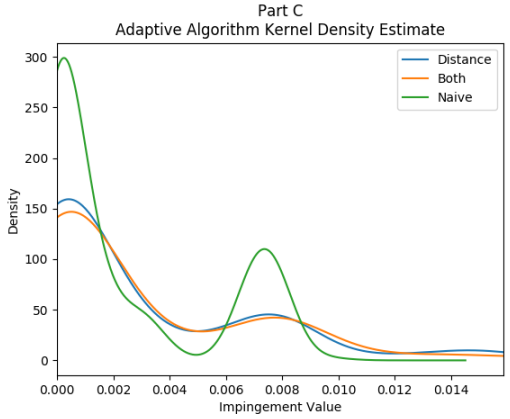

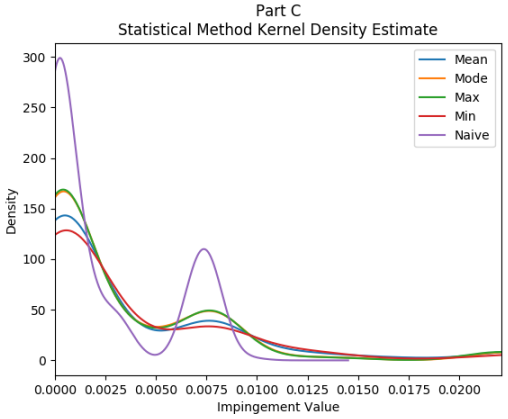

3.8. APPENDIX B – Kernel Density Estimates (Cont.)

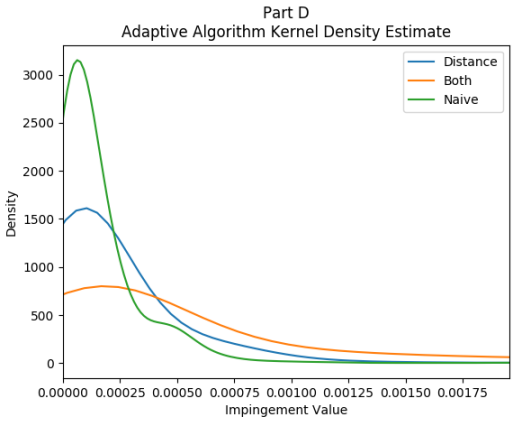

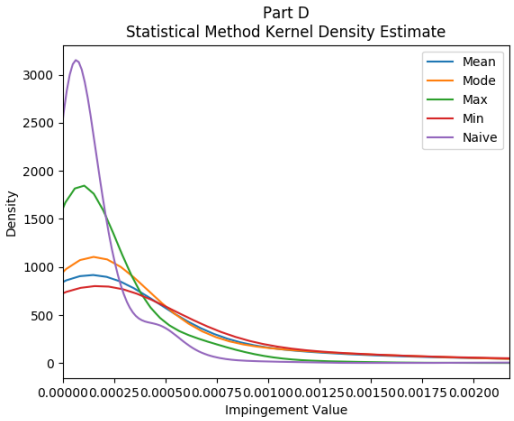

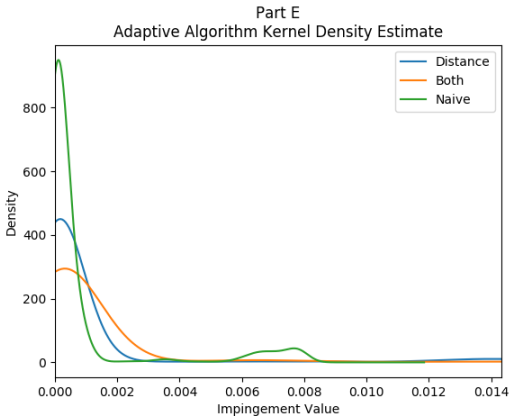

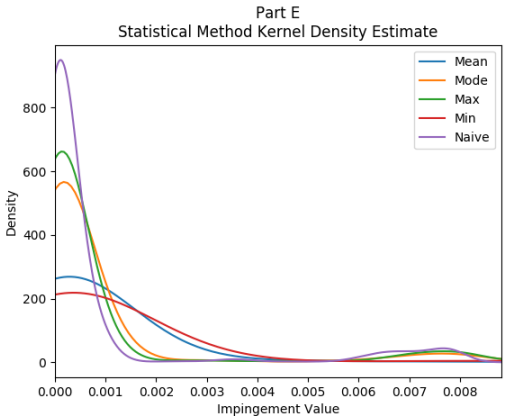

3.9. APPENDIX C - Histograms

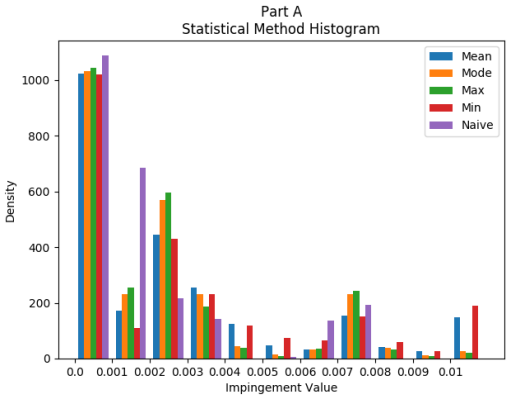

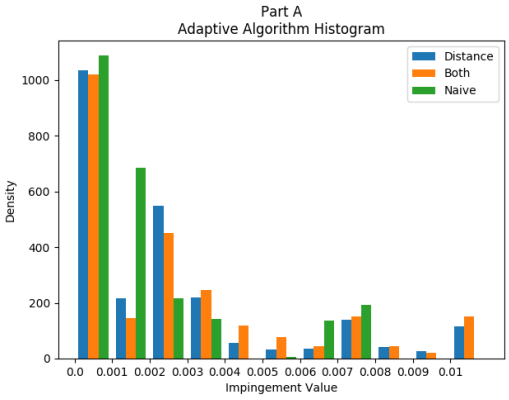

3.9. APPENDIX C – Histograms (Cont.)

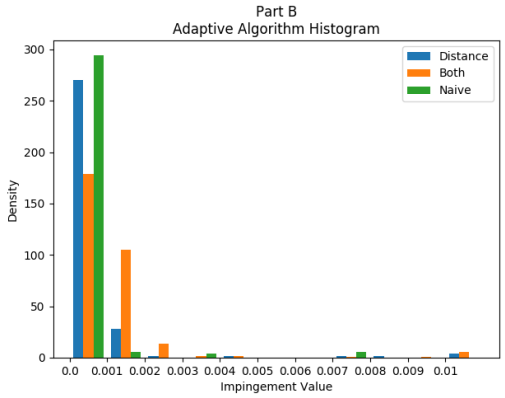

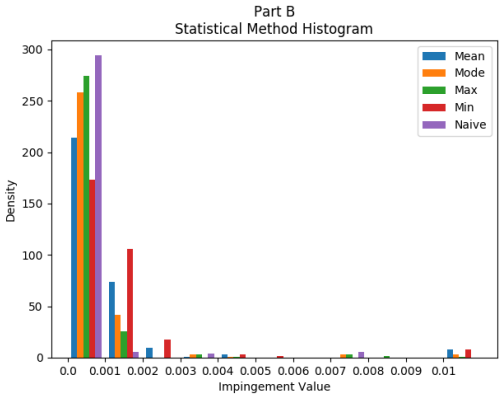

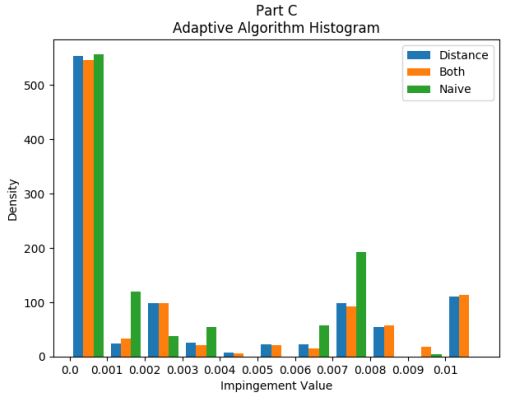

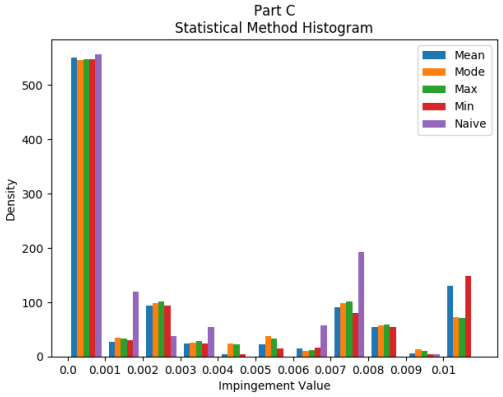

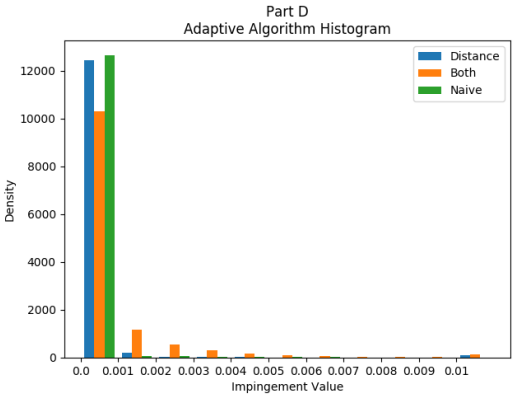

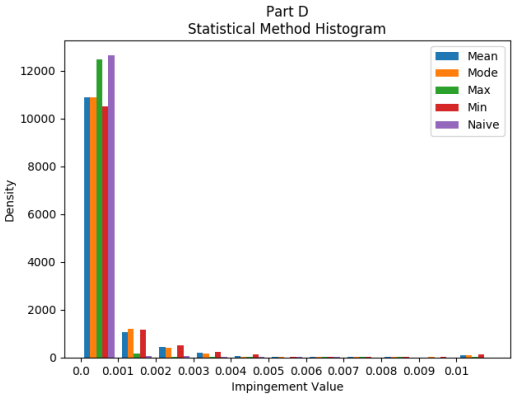

3.9. APPENDIX C – Histograms (Cont.)

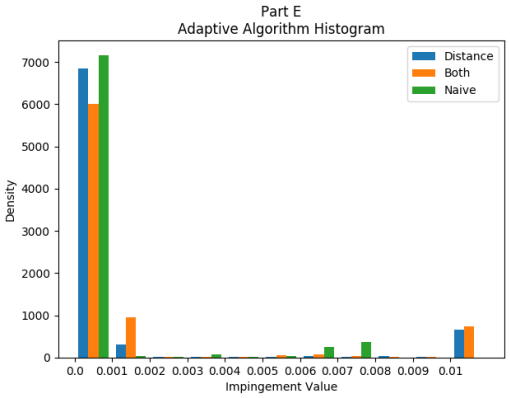

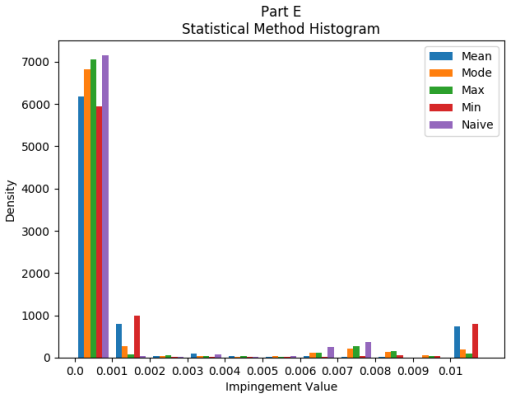

3.10. APPENDIX D – Versus Plots

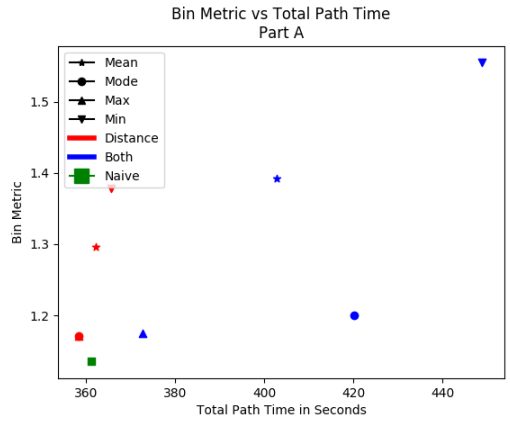

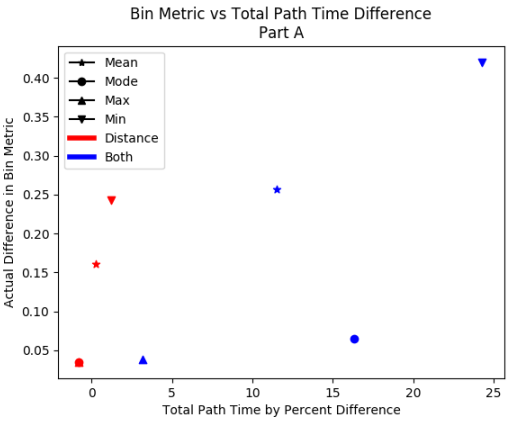

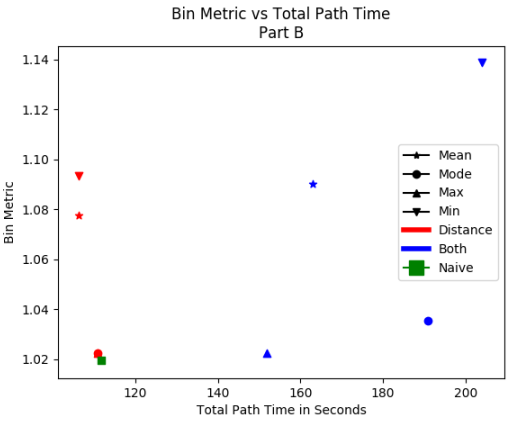

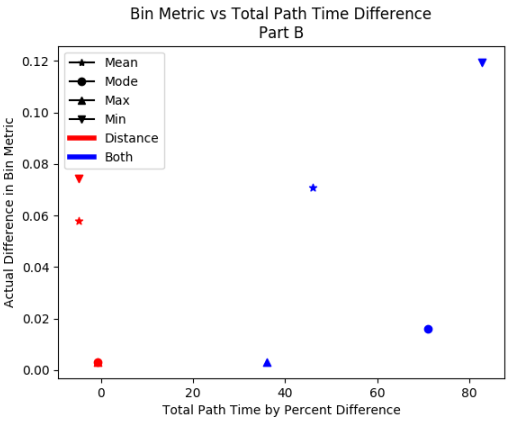

3.10. APPENDIX D – Versus Plots (Cont.)

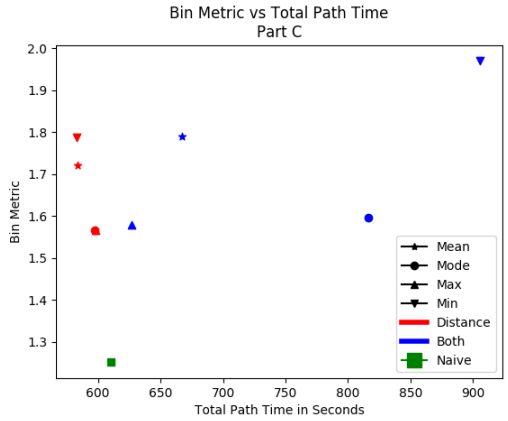

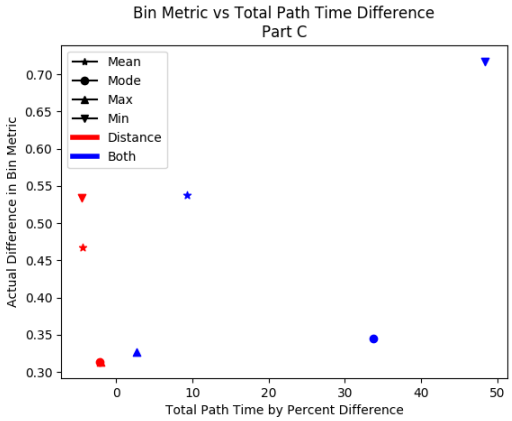

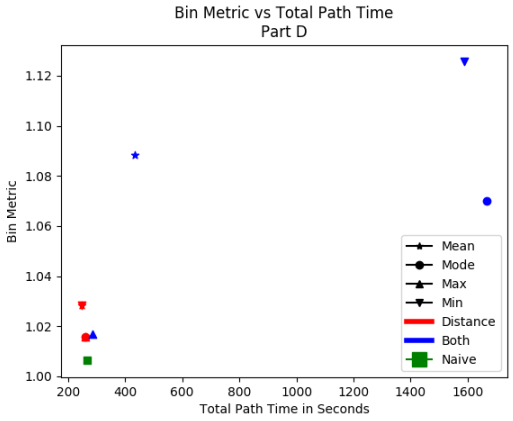

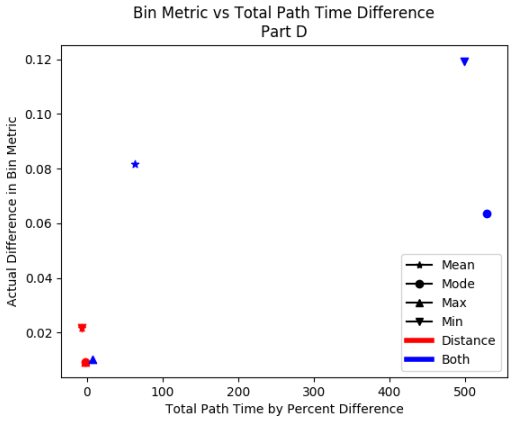

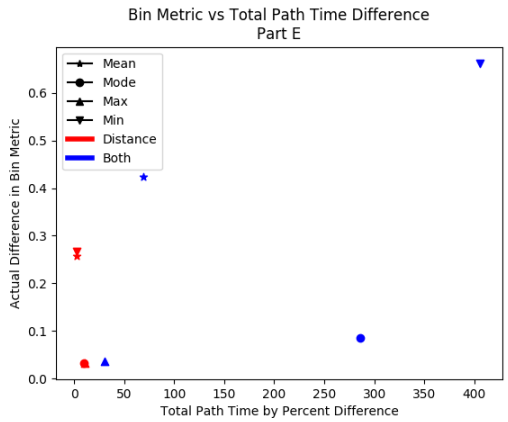

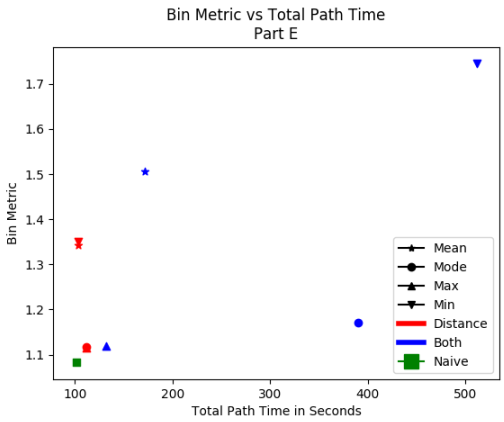

3.11. APPENDIX E – Individual Treatment Results

3.11.1. Part A - Test Part

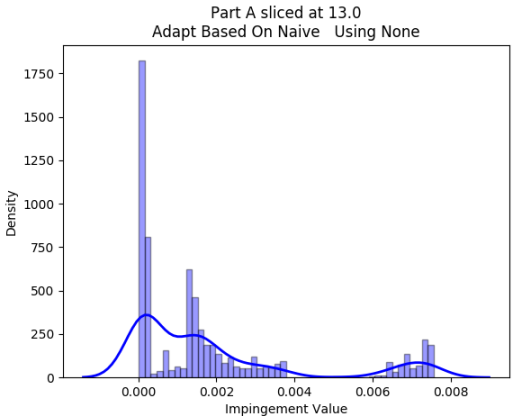

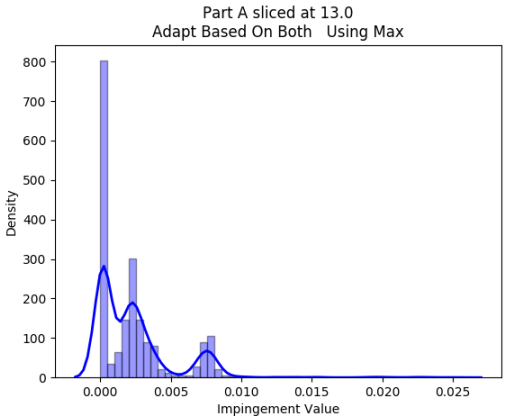

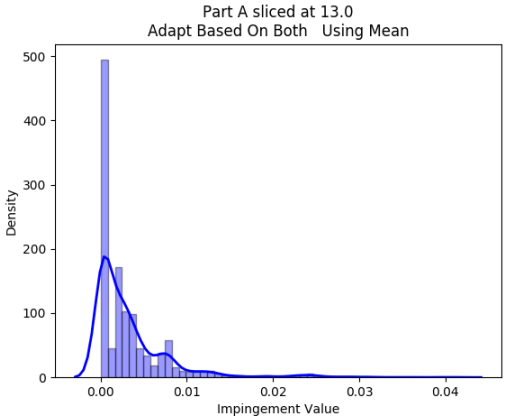

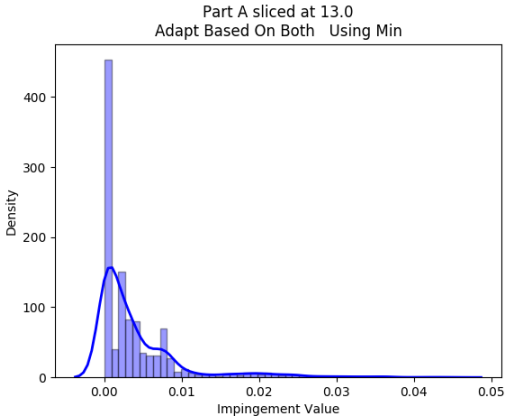

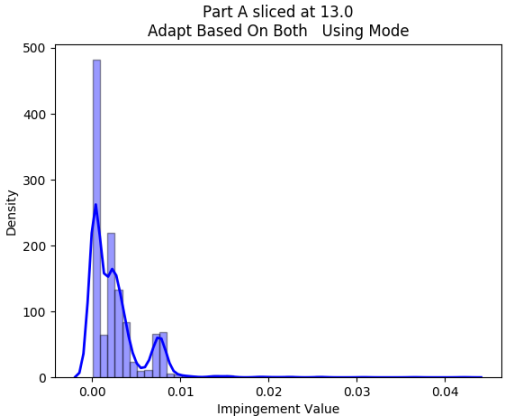

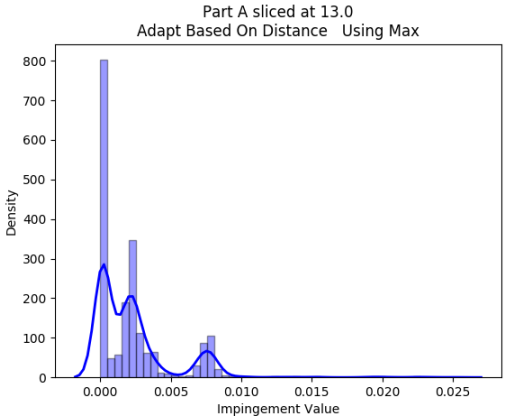

3.11.1. Part A - Test Part (Cont.)

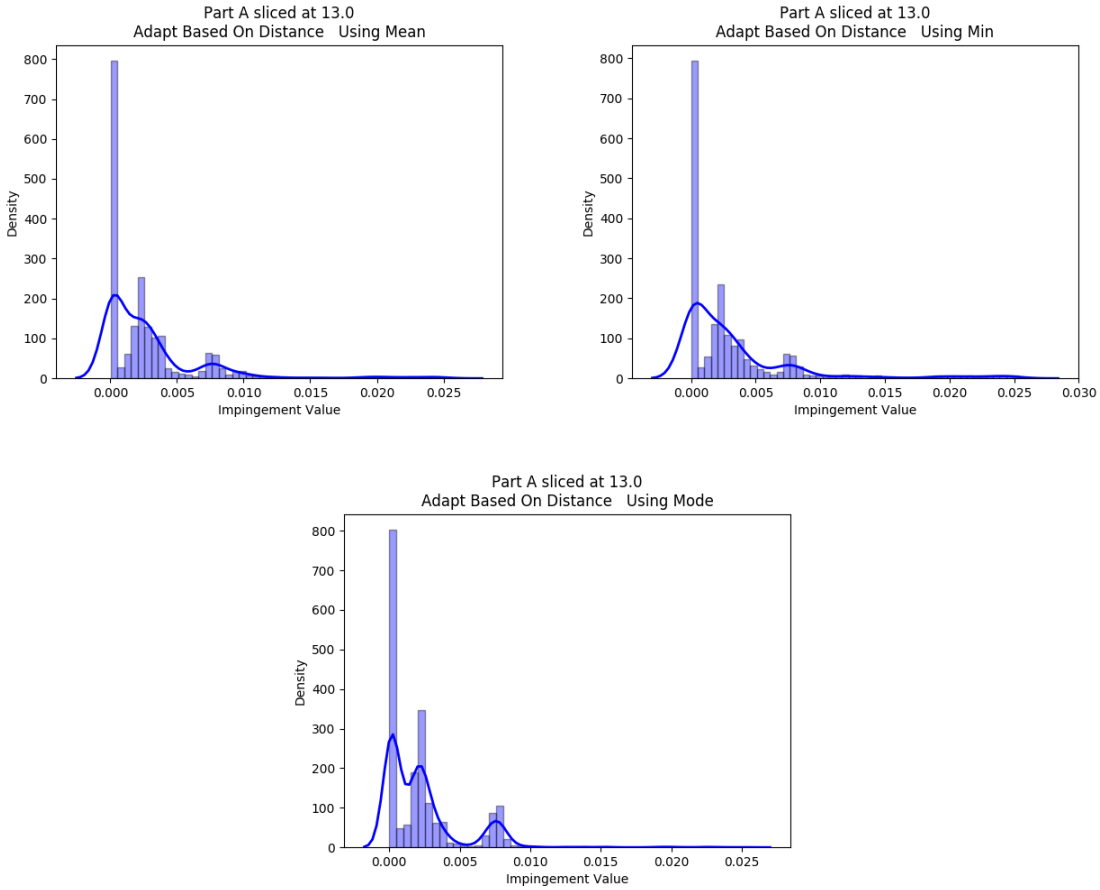

3.11.2. Part B – Incidence Test

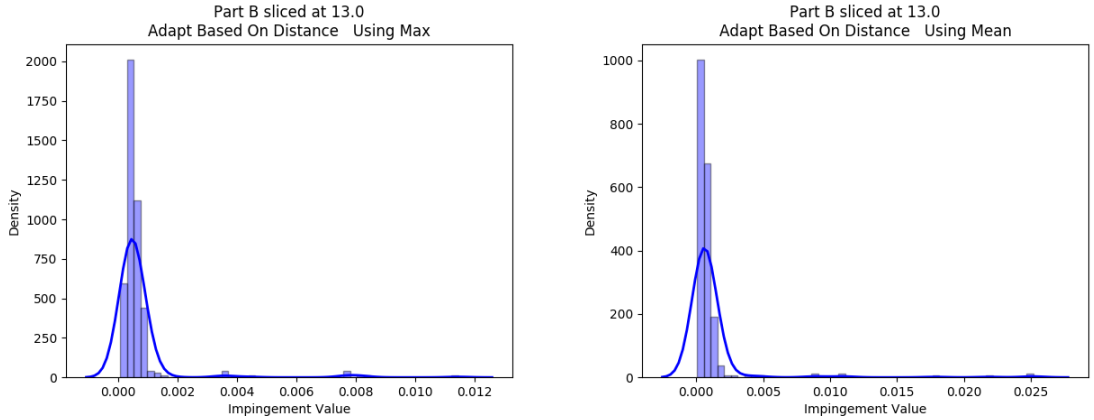

3.11.2. Part B – Incidence Test (Cont.)

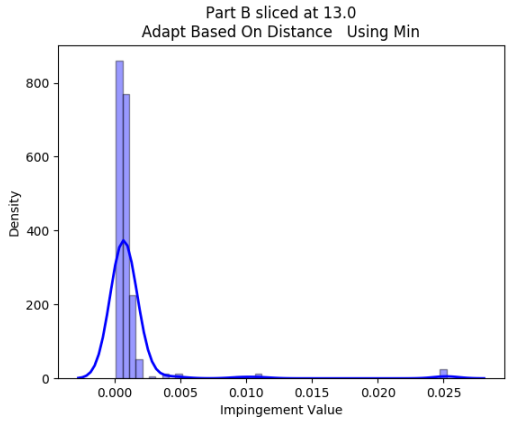

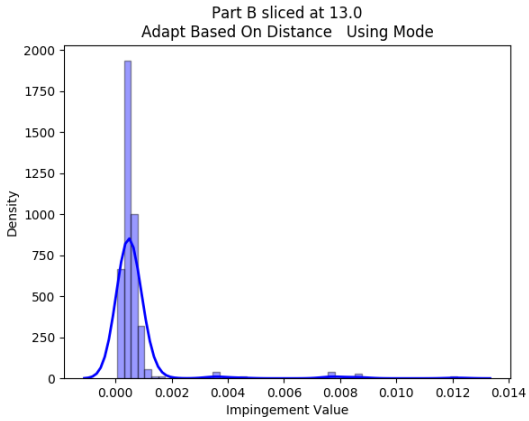

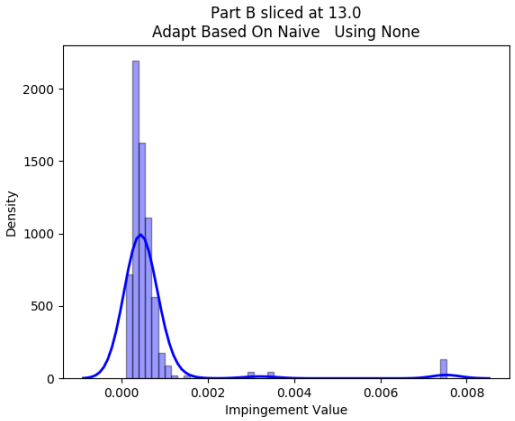

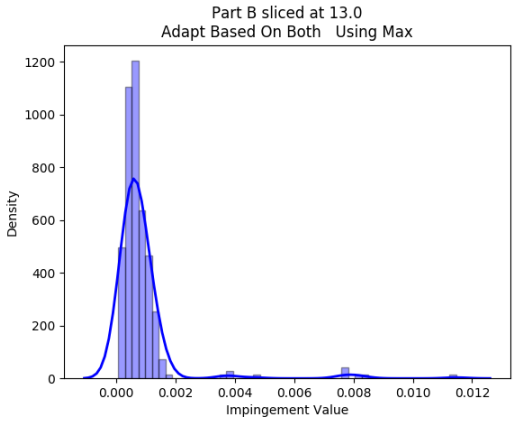

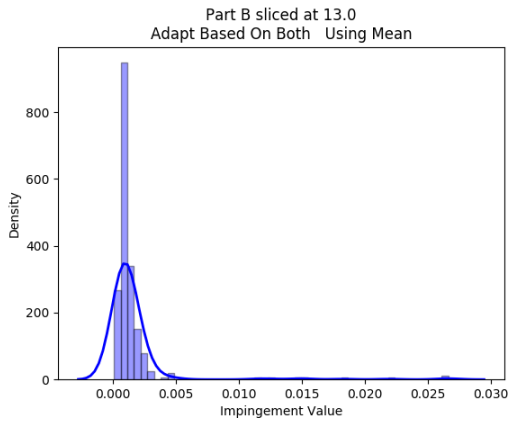

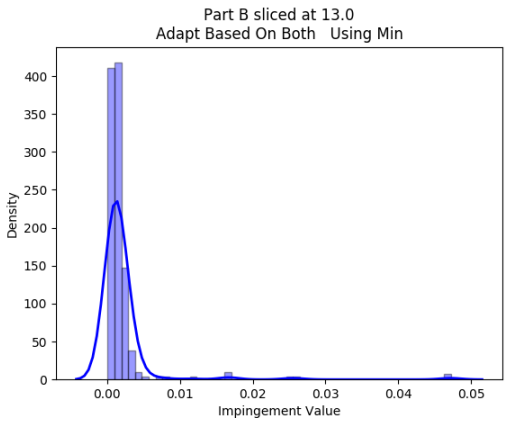

3.11.2. Part B – Incidence Test (Cont.)

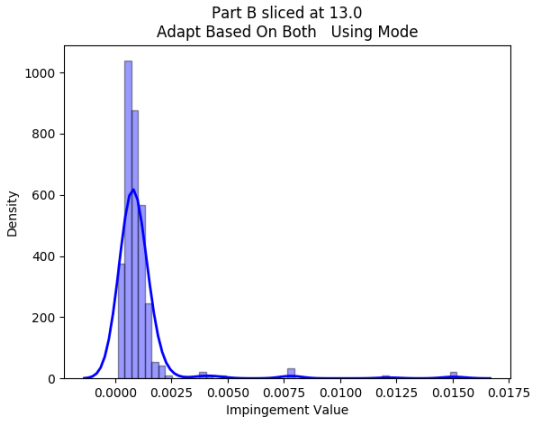

3.11.3. Part C – Solid Wheel Upright

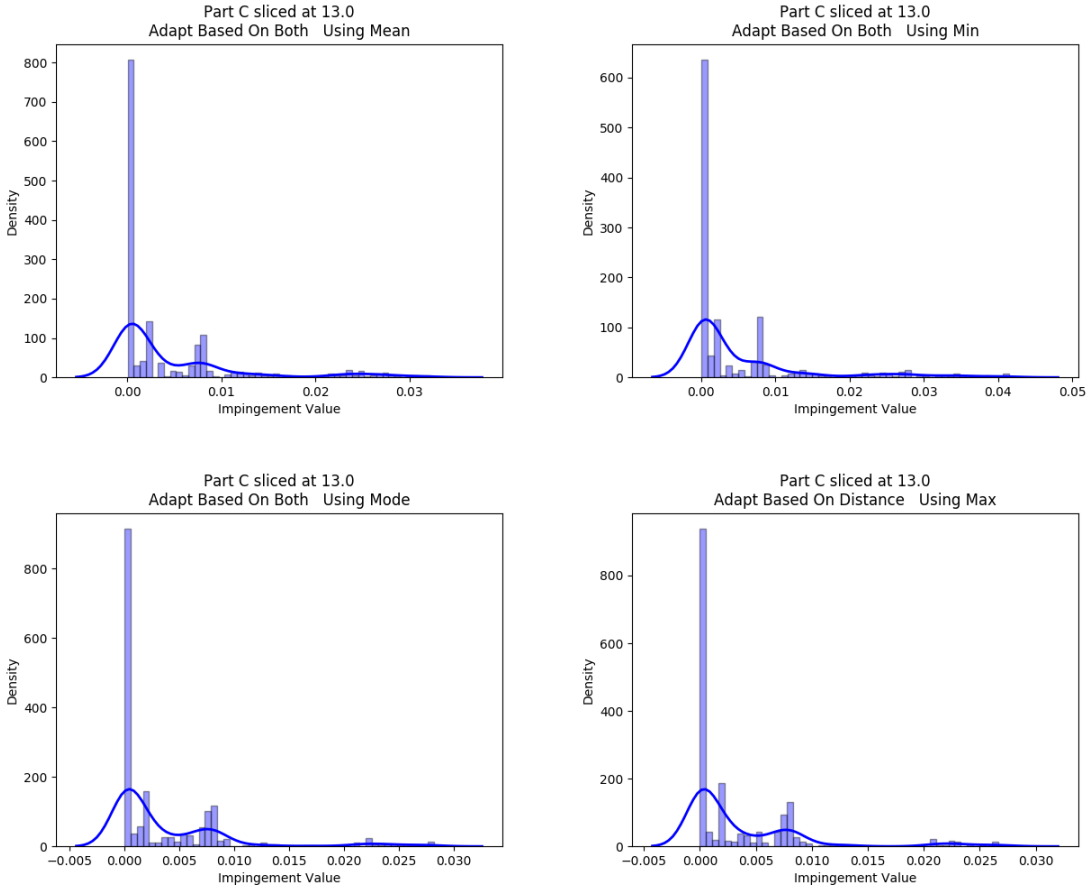

3.11.3. Part C – Solid Wheel Upright (Cont.)

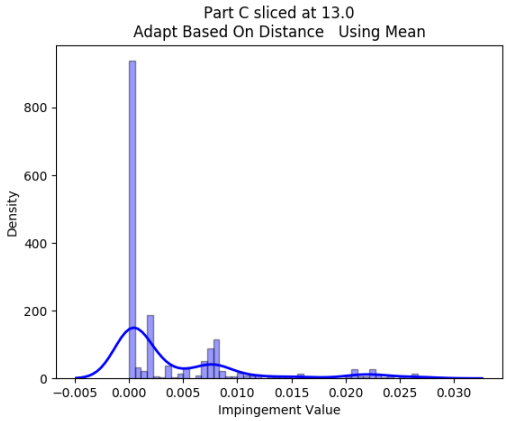

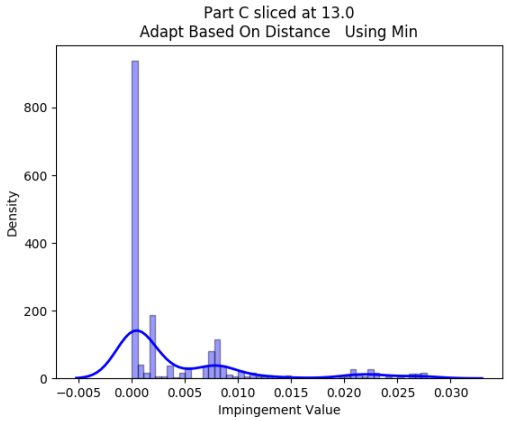

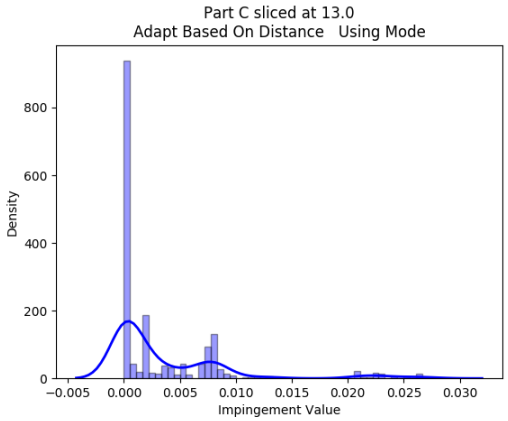

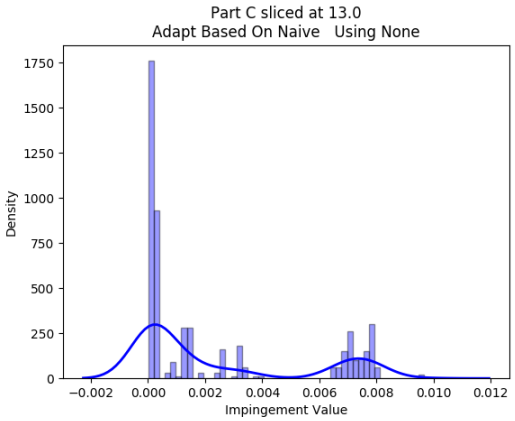

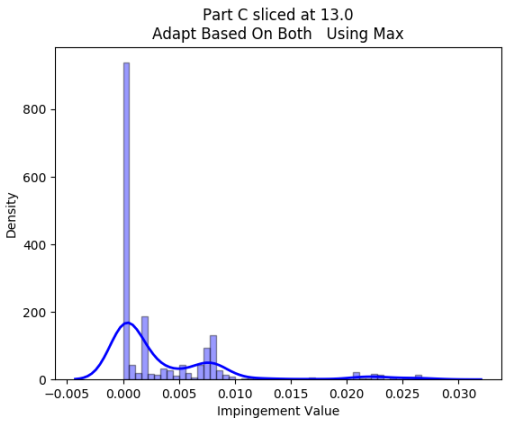

3.11.4. Part D – Blade Reduced

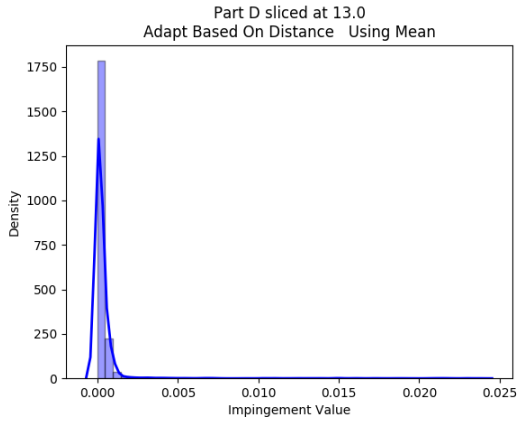

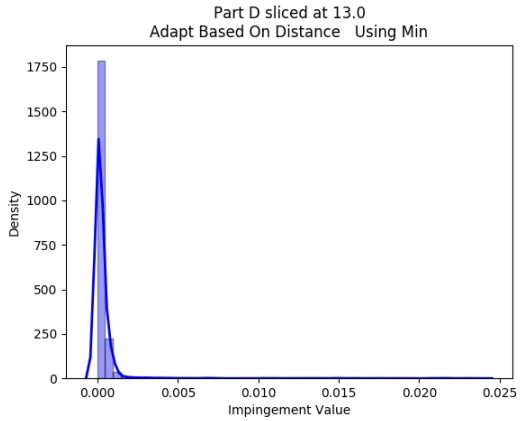

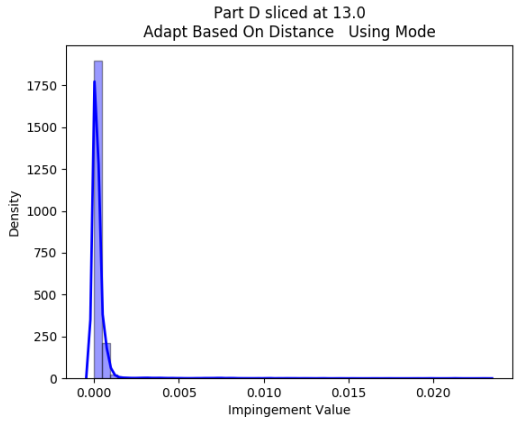

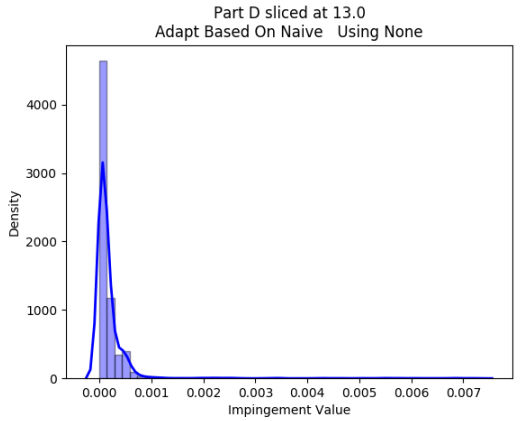

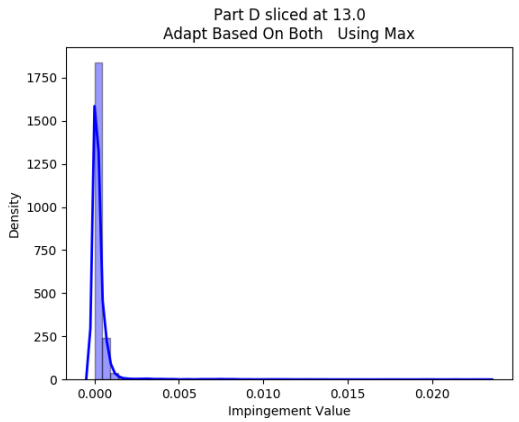

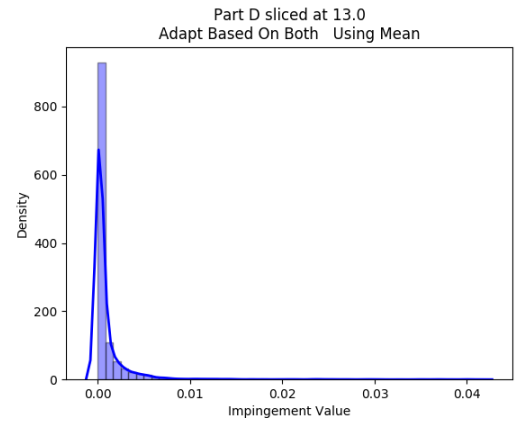

3.11.4. Part D – Blade Reduced (Cont.)

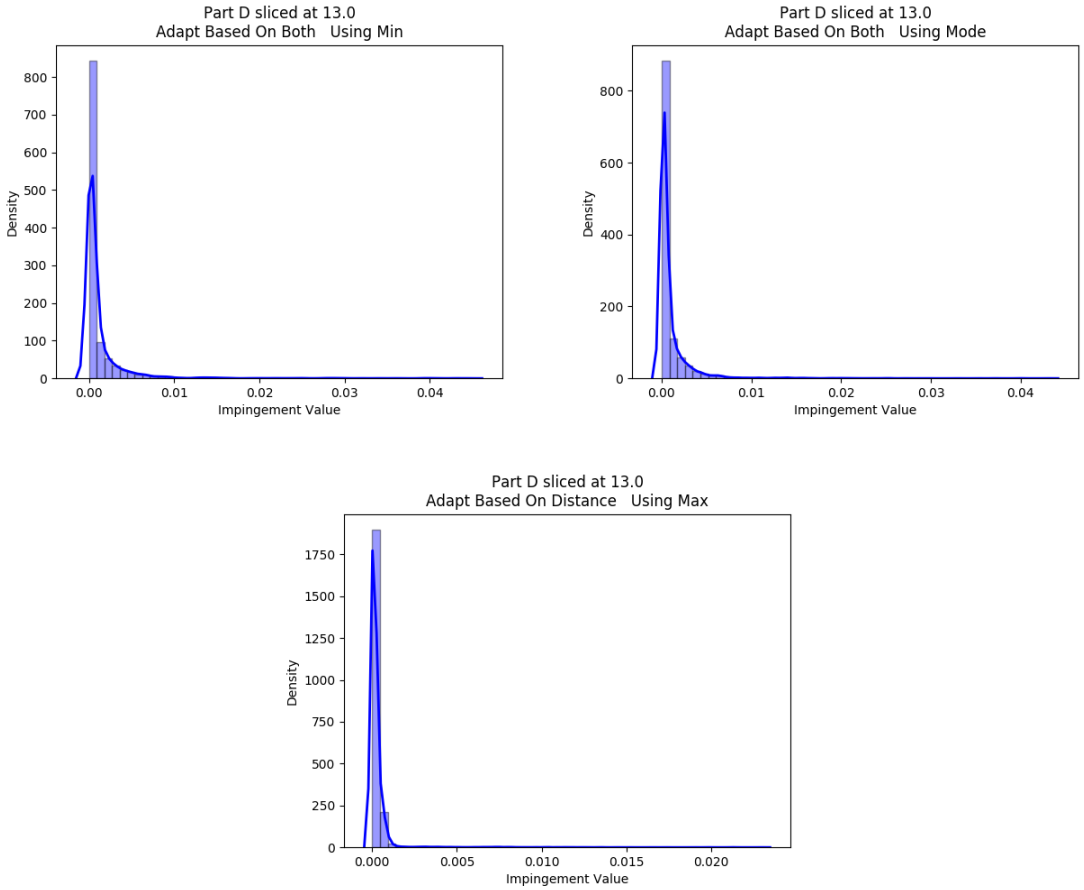

3.11.5. Part E – Wing Section Reduced

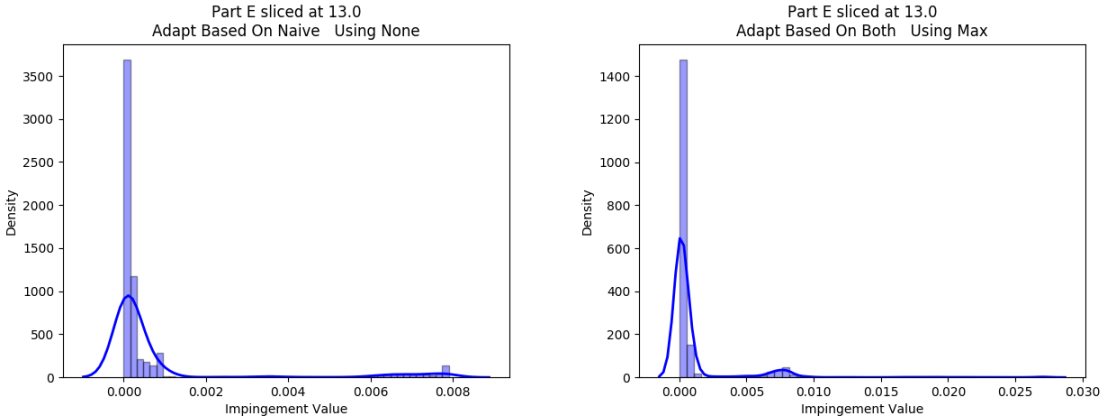

3.11.5. Part E – Wing Section Reduced (Cont.)

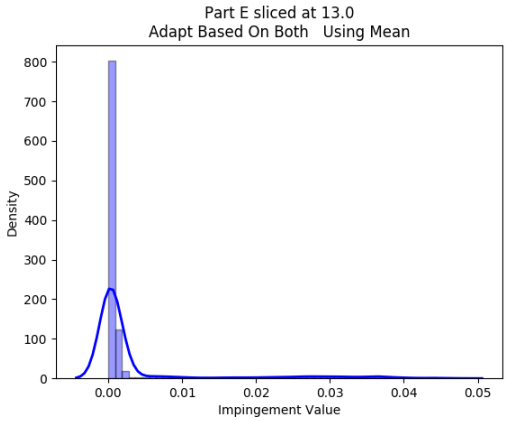

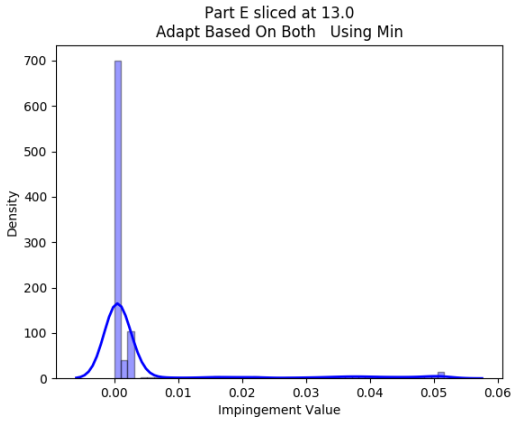

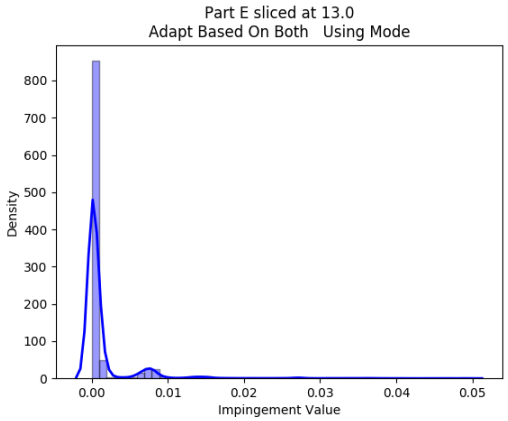

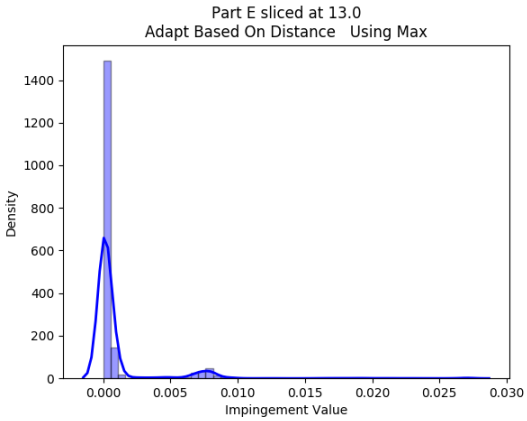

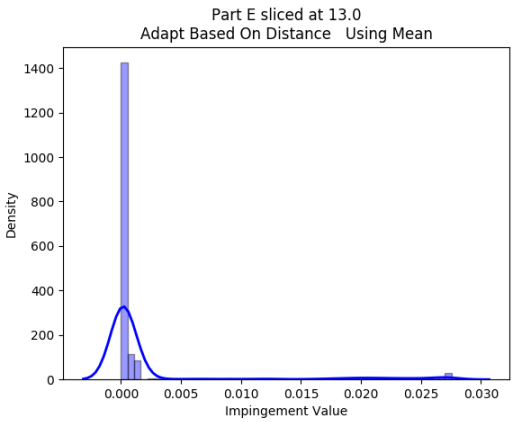

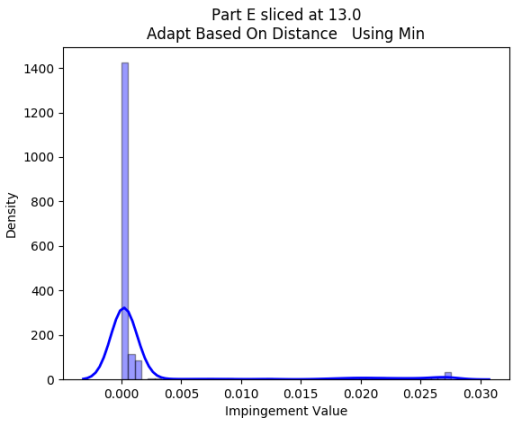

3.11.5. Part E – Wing Section Reduced (Cont.)

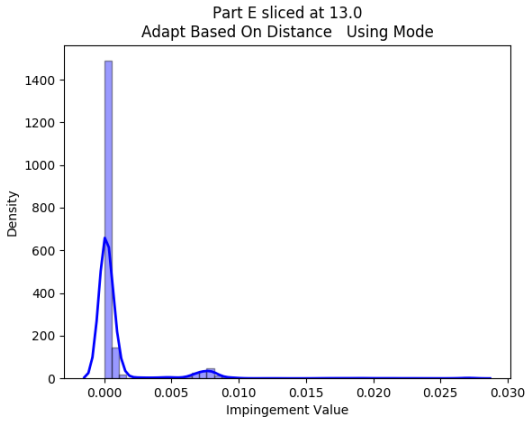

3.12. APPENDIX F – Nomenclature Table

$A =$ ordered set of unique surface points $\boldsymbol{a}$

$\boldsymbol{a}_{fi} =$ intersecting surface points created from facet *f*

B_i = set of all points mapped to bin *i*

$B_s =$ set of all bins on slice *s*

$\widehat{\boldsymbol{b}}_i$ = segment normal of segment *i*

C = point cloud of the original part

$C_s =$ point cloud points effected by slice *s*

c = point in the original point cloud

d_O = offset distance

d_{AG_b} = aggregate distance value of all points in bin *b*

d_p = movement distance to $\boldsymbol{p}$

e_{fi} = interpolation percentage for side i of facet *f*

ε = limit on angular deviation for adjacent points

η = number of facets in a part

F_s = intersecting facets on slice *s* of the convex hull

f = facet of the convex hull

G = robotic trajectory

g = tool trajectory observation

H = convex hull of the part

$h_s =$ height of slice *s*

l_i = actual length of segment i

l_m = maximum allowable length of a segment

γ_c = impingement value of point *c*

m = appropriate number of slices for the convex hull or segments needed to meet the limit ε

$N =$ set of normal vectors associated with surface point $\boldsymbol{a}$

$\widehat{\boldsymbol{n}}$ = unit normal vector

P = ordered set of all path points $\boldsymbol{p}$

P_s = set of all points in slice *s*

$\boldsymbol{p} =$ end effector position

$\boldsymbol{p}_{\text{new}_j}$ = intermediary point *j* being added to the path in bin

$\Phi_s =$ ordered set of all points and normal vectors in slice *s*

$\boldsymbol{\phi}_{fi}$ = vector between the lone vertex and the other two vertices

φ = set of $\boldsymbol{p}$ and $\boldsymbol{n}$

3.12. APPENDIX F – Nomenclature Table (Cont.)

$\varphi_{\boldsymbol{p}}$ = angular polar coordinate of the path point $\boldsymbol{p}$

$\varphi_{\min}$ / $\varphi_{\max}$ = extreme angular polar coordinates

ψ_b = distance adjustment value for each bin

ψ_{b_p} = adjustment value of point *p* in bin b

ψ_p = adjustment value of point *p*

$\boldsymbol{q}_{fiZ}$ = Z value of vertex *i* of facet *f* on the convex hull *H*

$\boldsymbol{q}_{fA}$ = lone vertex on one side of the slicing plane

$\boldsymbol{q}_{fBi}$ = vertex *i* opposite the lone vertex

R = ordered set of all orientation vectors $\boldsymbol{r}$

$\boldsymbol{r}$ = end effector orientation

S_{part} = slices selected as part of partial path

s = index of the slice

σ = offset percentage

T = ordered set of all time values *t*.

t = timestamp

Δt_p = movement time to $\boldsymbol{p}$

τ_{bc} = time adapted incidence value for point *c* in bin *b*

θ = angle of the spray cone

θ_{bc} = incidence value for point *c* contained in bin *b*

θ_{AG_b} = aggregate incidence value of bin *b*

u_f = number of vertices of facet *f* above the slicing plane

v_0 = base velocity of process

v_b = velocity of bin *b*

$\hat{\boldsymbol{v}}_i$ = unit vector between $\boldsymbol{p}_i$ and $\boldsymbol{p}_{i+1}$

w_A = slice thickness

w_O = offset width

Ξ = set of all consecutive adjacent points that are colinear to all points

ξ = set of consecutive adjacent points for a specific point

Z_{max} / Z_{min} = extreme values in the Z axis

ζ = bin metric of a part

4. FINAL CONCLUSIONS

Taking these two papers together, a groundwork was laid for the implementation of a collaborative robotic pressure washing work cell. The framework described in chapter 2 sets a standard for system design and infrastructure and the path planner described in chapter 3 can be utilized in both the initial planning and rework modules from the framework. In the process of developing both the framework and path planner, a prototype system was built to model the pressure washing work cell that inspired this project. Currently, the prototype system encompasses everything included in both papers except for the physical implementation of the work cell. The user is prompted to input the initial 3D data and input parameters before the adaptive path planner takes over and generates an initial path plan. After seeing the visualization, the user can select specific areas of the part for replanning or approve the path. If replanning is required, the user is again prompted for some input parameters and then the new replanned path is added on to the initial path or can replace it entirely.

Moving forward, work still needs to be done on developing better analysis techniques that more accurately model what facets are actually being covered by the path plan, especially with regards to complex geometries that may hide pieces of the part from the sprayer. There is also a need for even more advanced path planners that can dynamically change the structure of the path when the adaptive measures cause once covered pieces to go uncovered. Aside from the research-based advances, the obvious next step is to turn the virtual prototype into a physical prototype. To do this, two things need to happen. First, the resulting path from the path planner needs to be checked and reconfigured to reflect the physical limitations of the robot performing the task, and second, there needs to be some system in place to gather the 3D data from the part relative to the robot.

In summary, the Army's need to remove operators from the pressure washing work cell led to the creation of a collaborative task specification system designed to handle a wide variety of novel parts requiring reliable one-off path planning, which in turn led to the development of an adaptive path planning algorithm for better quality toolpaths.